12-2020

Influence of Liquid Height on Pool Boiling Heat Transfer

Maharshi Y. Shukla
ms1235@rit.edu

RIT

Influence of Liquid Height on Pool Boiling Heat Transfer

by

Maharshi Y. Shukla

A Thesis Submitted in Partial Fulfilment of the Requirements for the Degree of Master of Science in Mechanical Engineering

Thermal Analysis, Microfluidics, and Fuel Cell Lab,

Department of Mechanical Engineering

Kate Gleason College of Engineering

ROCHESTER INSTITUTE OF TECHNOLOGY

Rochester, New York

December 2020

Influence of Liquid Height on Pool Boiling Heat Transfer

By: Maharshi Y. Shukla

A Thesis Submitted in Partial Fulfilment of the Requirements for the Degree of Master of Science in Mechanical Engineering

Department of Mechanical Engineering

Kate Gleason College of Engineering

Rochester Institute of Technology

Approved by:

Dr. Satish Kandlikar

Thesis Advisor *Date*

Department of Mechanical Engineering

Dr. Jason Kolodziej

Thesis Committee Member *Date*

Department of Mechanical Engineering

Dr. Robert Stevens

Thesis Committee Member *Date*

Department of Mechanical Engineering

Dr. Stephen Boedo

Department Representative, Thesis Committee Member *Date*

Department of Mechanical Engineering

Abstract

As technology advances due to continuous research, devices are becoming more compact, efficient, and powerful. Therefore, heat rejection from such devices becomes ever so critical to maximizing their potential. Compared to other heat extraction methods, boiling provides one of the highest heat transfer coefficients. The heat extraction due to the boiling process is limited to the Critical Heat Flux (CHF). At CHF, an insulating layer of escaping bubbles forms upon the surface to prevent boiling continuity. Subsequently, the surface temperature increases uncontrollably, leading to a system failure. Hence, the elevation of CHF is critical to boiling enhancement. Improvements to the heat transfer process can be made with either surface manipulation or liquid manipulation. Based on previous studies, it is found that the removal of bubbles from the heater surface is critical to enhancing performance. Therefore, it is hypothesized that if a bubble can be encouraged to reach liquid-gas the interface quickly, gains in the boiling performance can be achieved. Due to the vapor bubble's movement in liquid bulk, it becomes critical to understand the influence of liquid height on pool boiling for enhancement. While pool boiling enhancement using heating surface modification is extensively studied and documented, there is a research gap between understanding the effect of liquid height at high heat fluxes. Thus, this study tries to evaluate the influence of liquid height on pool boiling performance at higher heat fluxes and identify the underlying bubble movement mechanism. It is observed that as CHF increases with liquid height. Moreover, it is observed that bubble movement is more effortless at low liquid height resulting in higher HTC. On the other hand, larger liquid height provides improved rewetting of the surface resulting in higher CHF. Upon analysis of high-speed recording of the escaping bubbles, it was observed that the maximum heat transfer coefficient is observed when the liquid height is about four times the height of the departing bubble diameter.

Acknowledgment

I would like to express my sincere thanks to Dr. Satish Kandlikar for providing the opportunity to research this unexplored field of engineering in the Thermal Analysis and Microfluidics Laboratory. His continuous support, guidance, and motivation have helped me learn about the theory of the subject and understand the details of the topic.

Besides my advisor, I would like to thank my committee members, Dr. Jason Kolodziej and Dr. Robert Stevens, for joining the committee. I sincerely appreciate their effort to review and scrutinize my research. Their valuable feedback has made the research more meaningful for society.

I would like to thank Dr. Michael Schrlau and Jill Ehmann, and everyone in the ME office for their continuous support and guidance. I would also like to thank the Machine Shop faculty, Jan Maneti, Craig Arnold, and Ricky Wurzer, for their help and guidance in fabricating the setup and chip.

Moreover, I would like to thank Aniket Rishi, Aranya Chauhan, and all the members of the TAMFL for helping me cope with the various experimental procedures and laboratory instruments. Their constant guidance has helped me throughout to troubleshoot and understand the issues faced.

Finally, I would like to thank my family for their constant support throughout the thesis. They have always encouraged me to pursue my interests.

Contents

List of Figures

List of Tables

Abbreviation

$B_{q"}$	Bias uncertainty corresponding to heat flux
D_b	Bubble diameter (mm)
E%	Error percentage corresponding to heat flux
h	Heat Transfer Coefficient (W/m^2-K)
H	Height of liquid pool (mm)
H*	Non dimensional height (mm)
K_{Cu}	Thermal Conductivity (W/m-K)
$P_{q"}$	Precision uncertainty corresponding to heat flux
q"	Heat Flux (W/cm^2)
$T_{saturation}$	Saturation Temperature of water (°C)
$T_{surface}$	Temperature on the heating chip surface (°C)
T_1	Temperature recorded by thermocouple 1 (°C)
T_2	Temperature recorded by thermocouple 2 (°C)
T_3	Temperature recorded by thermocouple 3 (°C)
T_4	Temperature recorded by thermocouple 4 (°C)
T_5	Temperature recorded by thermocouple 5 (°C)
U_{Kcu}	Uncertainty corresponding to the thermal conductivity of copper
$U_{q"}$	Total uncertainty corresponding to heat flux
U_T	Total uncertainty corresponding to temperatures T_1, T_2, and T_3
U_x	Uncertainty corresponding to Vernier
X_1	Distance between thermocouples inside the heating chip and heating surface (mm)
ΔX	Distance between T_1 and T_2 and T_2 and T_3 (mm)

1.0 Problem Introduction

As technology is advancing due to continuous research, the inception of more compact, efficient, and powerful devices is observed. However, heat rejection from such devices becomes ever so critical in maximizing their potential, and hence efforts need to be laid to improve the current cooling techniques. Microelectronic devices, servers, supercomputers, power plants, and boilers are some of the equipment which can benefit from improved two-phase heat transfer across their respective boundary layers. Although being essential to the device's performance, cooling devices add to its cost and packaging. Hence, cost-effective means to find out better cooling techniques is the requirement of the hour. Out of all the various techniques applied to cool a device, boiling becomes the more effective one [1]. While single-phase heat transfer can only utilize specific heat, a two-phase heat transfer mechanism like boiling takes advantage of the latent heat of evaporation and specific heat, making it a more efficient form of heat transfer. Boiling is a phase change process that takes away heat in high fluxes as it converts the liquid into vapor. The boiling process consists of nucleation in the liquid cover cavities on the heater surface, bubble inception, bubble growth, and bubble departure from the heating surface to the liquid-gas interface and subsequent bubble collapse. Figure 1 represents the Pool Boiling curve first proposed by Nukiyama in 1934[2].

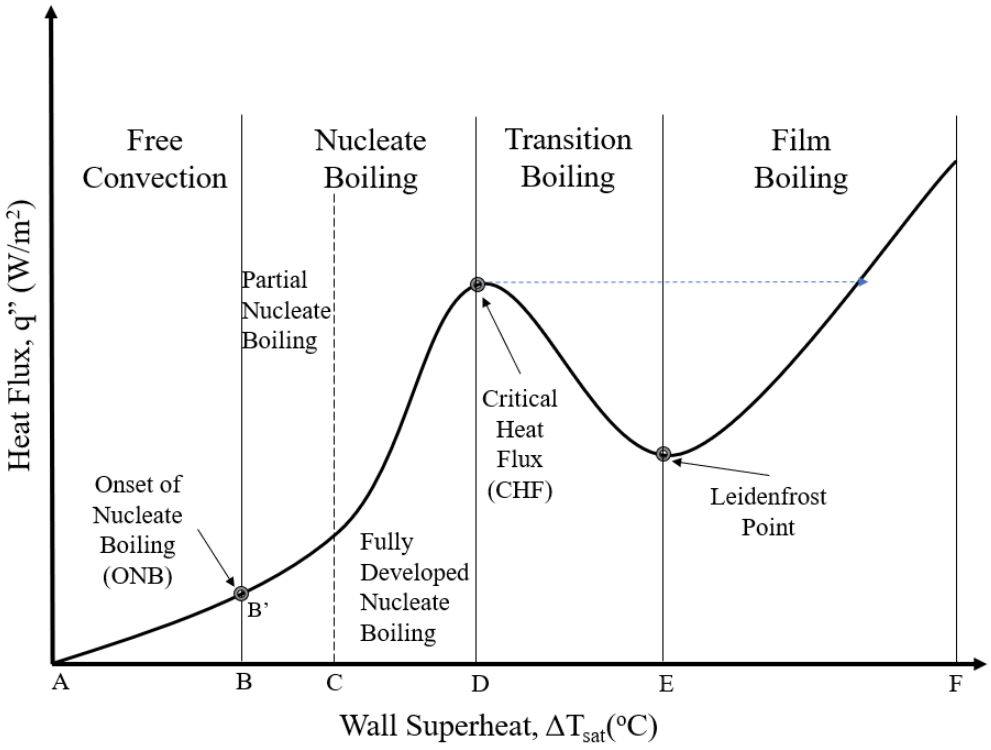

Figure 1 Pool Boiling Curve

Figure 1 shows the pool boiling curve that is a graph showing the relation between wall superheat on the horizontal axis and heat flux on the vertical axis. Nukiyama[2] chose to put heat flux on the vertical axis even though it was an independent variable in most pool boiling experiments with an electrically controlled heater. The heat flux is given in terms of $W/m^{2,}$ and wall superheat given in terms of °C. The pool boiling curve can be bifurcated into four regions, free convection region, nucleate boiling region, transition boiling region, and film boiling region. Furthermore, the nucleate boiling region can be sub-classified into the partial nucleating boiling region and fully developed boiling region. Moreover, the pool boiling curve defines three critical phenomena observed in boiling: the onset of nucleate boiling, critical heat flux, and Leidenfrost point. The pool boiling curve is discussed in detail below.

1.1 Free Convection Region

In the beginning, the water and heating surface is at Standard Temperature and Pressure (STP) conditions. As heat flux is provided to the heating surface, the heating surface temperature starts to rise, which heats the liquid above. As we further increase the heat, the water slowly heats up as we observe free convection region wherein both surface temperature and heat flux increase to reach the condition of Onset of Nucleate Boiling (ONB) until which no boiling bubbles are observed and the liquid pool only follows convective current to circulate. The Onset of Nucleate Boiling is the point where nucleating bubbles appear on the heater surface.

1.2 Nucleate Boiling Region

The onset of Nucleate Boiling is the gateway to the nucleate boiling region. As the bubble present on the heating surface starts to develop and detach, more heat is carried away by the liquid, and hence a substantial increase in heat flux is observed against smaller increments in wall superheat. Initially, isolated bubbles start to depart from the heating surface represented by a partial nucleate boiling region between regions B and C, as shown in Fig. 1. Further increasing the supply of heat flux to the heating surface, the vapor bubble grows in size and starts coalescing, and consequently, fully developed nucleate boiling is observed as seen between regions C and D. In this region, the coalesced bubbles form a column-like structure above the heating surface carrying a large amount of heat with them.

1.3 Transition Boiling Region

Upon further increasing the heat flux, critical heat flux is attained. Critical heat flux is the condition at which the vapor bubbles form such a large volume that they cover the heating surface. This

cover of the vapor bubble atop the heating surface and prevents the re-wetting of the heating surface and subsequently limits the process of boiling. Thus, the temperature of the heating surface starts to increase rapidly. Beyond critical heat flux, the boiling regime jumps to the film boiling region. CHF can lead to overheating of critical surfaces, which can lead to catastrophic consequences. Many boiling water reactor powerplants have witnessed failures due to boilers reaching CHF condition. However, when the heat flux is reduced from the film boiling region, the heating surface temperature reduces and follows the contour, as shown in the region between D and E. While the temperatures of the heating surface area reducing, a point called Leidenfrost point is observed. At Leidenfrost point, the heating surface's excessive temperatures form a layer of vapor atop which liquid can stay afloat. As heat flux is decreased, the lowering temperatures allow the breaking up of vapor bubbles, and re-wetting of the heating surface becomes possible again. Consequently, the boiling regime jumps back to the nucleate boiling region.

1.4 Film Boiling Region

To return to nucleate boiling from film boiling, heat flux needs to be reduced. However, since the heater surface is significantly hotter than the water's saturation temperature, the Leidenfrost effect is observed in which a vapor film acts as an insulator between the heating surface and liquid bulk to prevent boiling. Eventually, upon gradual cooling of the heating surface, the plot can be traced back to the nucleate boiling region following a jump from the Leidenfrost point to the left on the nucleate boiling curve at the same heat flux.

Hence, to improve the boiling performance, a reduction in wall superheat in the nucleate boiling region, an increase in CHF, or both are desired. To achieve it, researchers and scientists have focused mostly on pool boiling enhancement through surface modification or with the application

of liquid additives such as nanoparticles or surfactants. However, not much effort has been put into understanding the influence of bulk liquid height on pool boiling. Since boiling is the heat transfer process between a solid surface and a liquid in contact, researching the liquid behavior while the interaction becomes a crucial aspect. The work of fellow researchers in the field has been a thorough guide to bolster the underlying idea.

2.0 Literature Review

The following sections will briefly discuss the relevant work done by other researchers to understand the influence of liquid height on pool boiling heat transfer, the scaling of heater size, pool boiling enhancement, and liquid supply to the heater surface vapor extraction.

2.1 Study at Low Liquid Height

Matsuoka et al. [3] conducted a study to find the effect of liquid height on heat transfer of nucleate boiling on Horizontal Heating Surface between the liquid heights of 5 mm and 60 mm for a heat flux of only 3 W/cm^2. Since the study was conducted at extremely low heat flux and did not conduct study below 5 mm of liquid height, Nishikawa et al.[4] in 1966 further elaborated on their work and studied nucleating pool boiling heat transfer at low liquid height. The experiments were conducted on three kinds of heating surfaces and different liquids in the range of liquid levels from 1 mm to 30 mm. The authors' objective is to investigate the mechanism of boiling heat transfer in the liquid at a low level. The authors used a brass circulate plate, a copper cylindrical block, and a rectangular copper plate for their experiments. The authors define the liquid level as the distance between the heater surface and the liquid-atmosphere interface. The authors carried out the experiments at constant heat flux, changing the liquid level by subtracting the liquid through a siphon.

Figure 2 shows the experimental setup used by the authors in which a heating water jacket protects the test setup. The water inside the test setup is condensed and supplied back to the setup using a condenser. A heater element heats the heating surface, and thermal losses from other directions are prevented using glass wool. The liquid height is measured from the top of the heating surface to the free liquid-vapor interface.

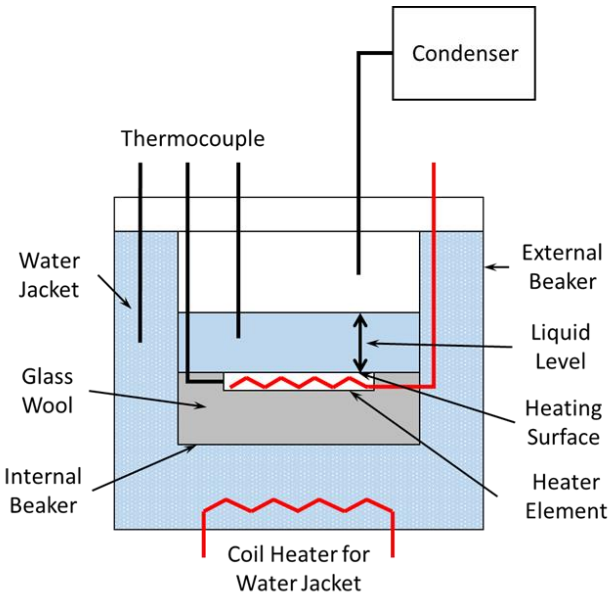

Figure 2. Pool Boiling Setup used by Nishikawa et al.

The authors assert that the aspect of boiling in which the liquid level is over 30 mm behaves similar to a regular pool boiling in which the boiling water circulates upwards in the center part and then flowing downwards along the walls of the vessel and finally flowing inward towards the center in the plane of the heating surface. At liquid levels less than 30 mm, water circulation is observed in

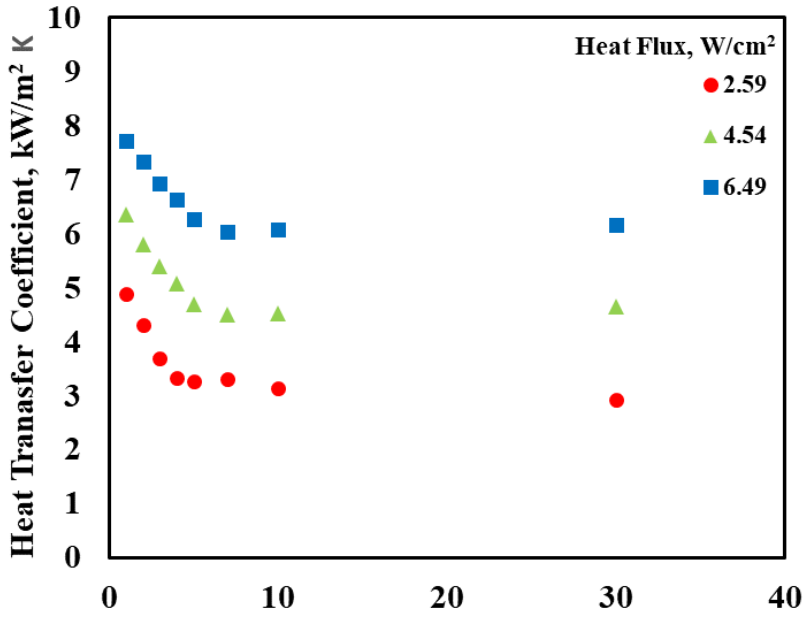

Figure 3 Heat transfer coefficient as a function of liquid height

a local convection manner. They observed an increase in nucleation sites with an increase in heat flux and decreasing liquid levels.

As a result of retardation of liquid recirculation due to lower liquid levels, more bubbles coalesced at the free liquid surface resulting in large vapor domes. However, the authors noted that these vapor domes do not play an essential part in the boiling heat transfer at low liquid levels. When comparing the influence of liquid height on pool boiling heat transfer, the authors observe that as liquid height decreases from 30 mm to 10 mm, the heat transfer coefficient remains reasonably constant. However, below 10 mm of liquid height, the heat transfer coefficient increases rapidly with reducing liquid height. Figure 3 plots the heat transfer coefficient as a function of liquid height for three distinct heat flux.

As seen in figure 3, the heat transfer coefficient is minimum at a liquid height of 7 mm. However, it is seen that these experiments are conducted at an extremely low heat flux. While the research provides vital pool boiling heat transfer insights at low liquid heights, it does not provide information about the influence of liquid height at higher heat fluxes, particularly near critical heat flux. Therefore, there is an open area to study the influence of liquid height on pool boiling heat transfer. The authors conclude that successful experiments could not be conducted due to unstable pool boiling performance below 1 mm of liquid height. Below 5 mm of liquid height, the increase in heat transfer coefficient was attributed to the local convection in liquid due to the generation and decimation of vapor domes along the liquid's free surface. However, it is the vapor domes that prevent stable boiling below 1 mm of liquid height.

The authors further observe that the impact of liquid height on pool boiling heat transfer decreases with increased heat flux. Figure 4 plots heat flux as a function of wall superheat for three different liquid height.

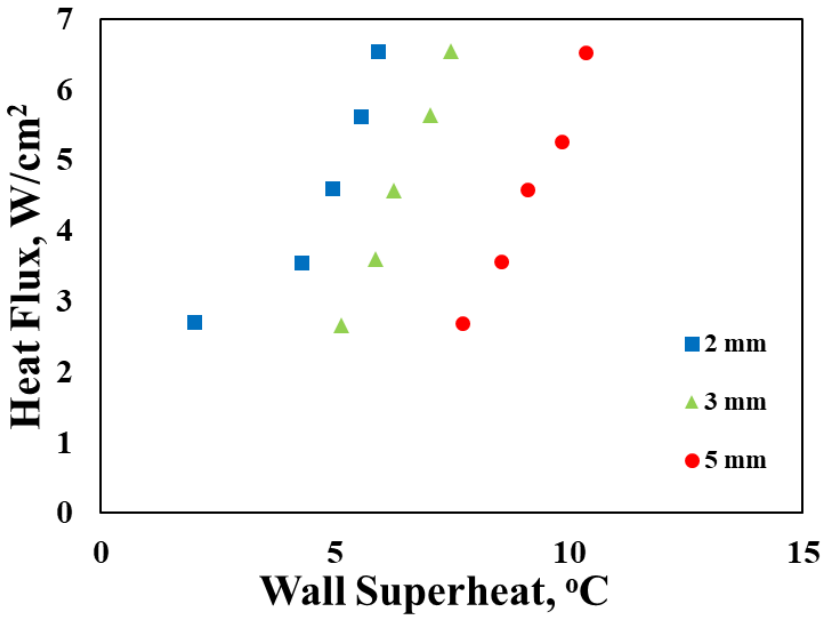

Figure 4 Pool boiling curve for 2 mm, 3 mm, and 5 mm liquid height

Figure 4 shows the pool boiling curve for 2 mm, 3 mm, and 5 mm liquid height. Since the experiments were conducted at low heat fluxes, the observations at higher heat fluxes, especially the near-critical heat flux condition, is unknown. It is observed that as liquid height increases, wall superheat increases at constant heat flux. However, it can be observed that with increasing heat flux, the influence of liquid height decreases.

2.2 Heater Size

Kwark Et al.[5] studied heaters with different surface area (0.75 cm x 0.75 cm, 1 cm x 1 cm, 1.5 cm x 1.5 cm, 2.0 cm x 2.0 cm). Upon experimentation, it is found that with an increase in heater size, the CHF reduces. The authors explain the fluid's resistance to meet the local hot spots to be the reason behind reduced CHF.

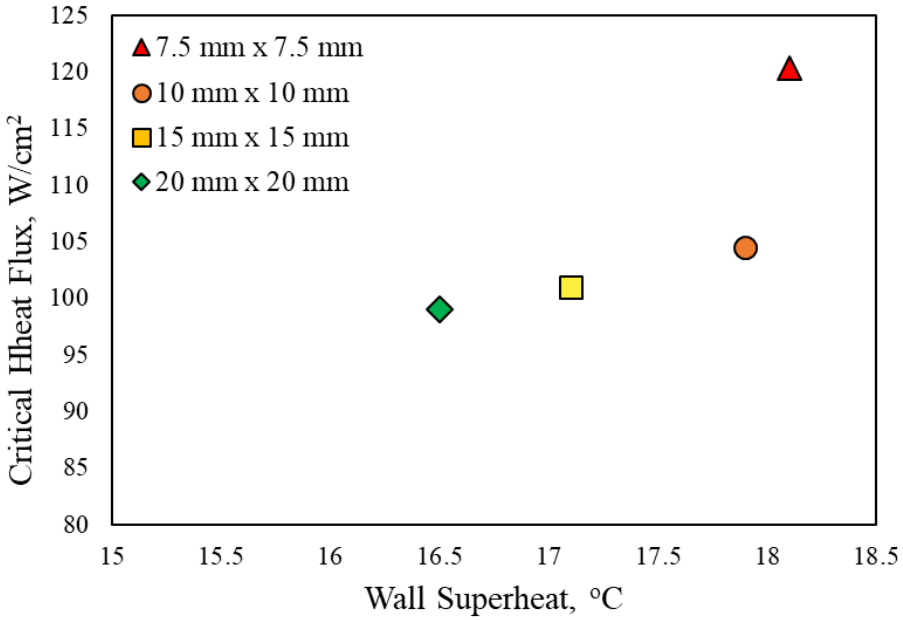

Figure 5 CHF as a function of heater size

Figure 4 shows the effect of liquid height on critical heat flux due to changes in heater size. As in the plot, the CHF reduces marginally as heater size is increased. The authors observe that with increasing heater size, though the nucleating density does not increase, the number of nucleating sites increase. Therefore, it becomes difficult for the working fluid to rewet the heating surface, and hence reduction in CHF is observed.

Based on previous authors'[6][7][8] observations and to keep consistency with the heating surface dimensions used by other researchers, the heating surface used in this study has 1 cm x 1 cm surface dimension to avoid scaling effects of heater size on critical heat flux.

3.0 Hypothesis

It is observed that pool boiling experiments are carried out at liquid heights that are significantly larger than the departure bubble diameter.

It is hypothesized that liquid height has a considerable effect on the pool boiling performance. The cumulative effect of bubble departure, bubble coalescence, and liquid height are responsible for vapor venting and corresponding rewetting of the heating surface through the liquid return.

The effect of liquid height is characterized in terms of departure bubble diameter since the bubble diameter is a characteristic length of pool boiling.

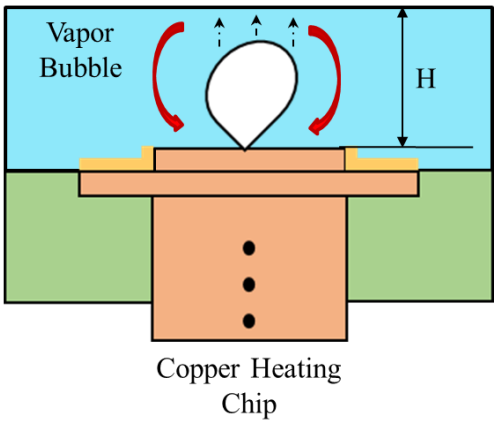

Figure 6 Vapor venting in low liquid height

As seen in figure 6, it is hypothesized that when the liquid height and departure bubble diameter become comparable, changes in the vapor venting mechanism will improve the heat transfer coefficient during pool boiling heat transfer.

4.0 Objectives

The literature review indicates the existence of dependence between liquid height and pool boiling performance. However, these studies have been conducted only at lower heat fluxes (less than 10 W/cm^2). Modern-day applications require high efficiency and high-power cooling systems, which tend to perform at higher heat fluxes. Therefore, it becomes critical to study the effect of liquid height at higher fluxes, i.e., near CHF conditions. Using high-speed videos, an analysis of the boiling performance will be conducted. It is hypothesized that pool boiling performance will improve at lower liquid heights because the less liquid height provides a shorter path for the vapor bubble to dump the heat into the atmosphere. Based on the hypothesis mentioned above, the following objectives are drawn for this research:

1. Characterizing pool boiling performance

- Creating a setup capable of feeding a continuous amount of water to the boiling region to maintain its bulk height over the heater surface
- Perform pool boiling tests to find out the influence of liquid pool height on heat transfer coefficient and critical heat flux

2. Bubble analysis

- Capture high-speed videos
- Analyze high-speed video
- Characterize the factors causing influence

5.0 Experimental Study

The literature review indicates the presence and working of different boiling mechanisms working at different liquid height. To further investigate the subject, a setup that can maintain liquid height while the entirety of the experiment is designed. The experimental setup consists of 3 main objects:

i. Copper Heating Chip

ii. Housing

iii. External Reservoir

The following sections enunciate the design, assembly, and working of the setup.

5.1 Copper Heating Chip:

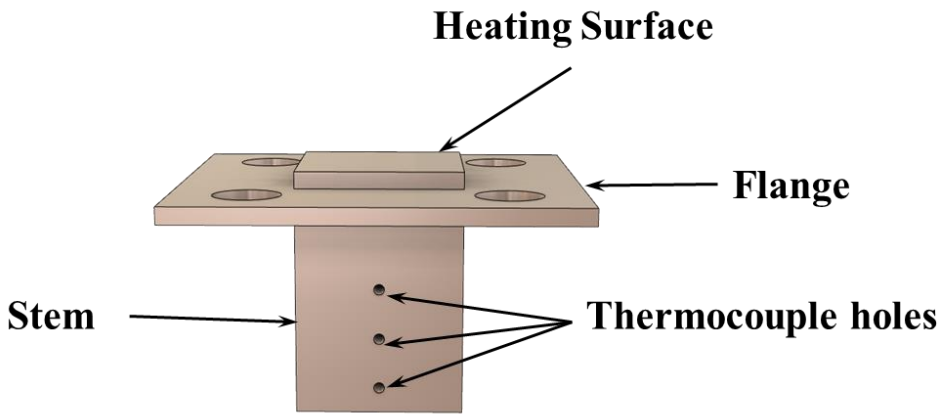

Figure 7 CAD model of the Copper Heating Chip

The copper heating chip provides the surface upon which boiling is desired while performing the experiments. The heating chip ensures 1D transmission of heat to the system and houses thermocouples for logging temperatures from various locations. As the name suggests, the heating chip is made from copper alloy 101 with 99.999% purity. The thermal conductivity coefficient and machinability of copper make it a suitable choice. The copper heating chip is manufactured using a CNC milling machine. After machining the chip, the chip's top surface is buffed to achieve the desired smoothness between 2 microns to 3 micros. Figure 7 shows the construction of the heating chip designed to perform the pool boiling experiments. The figure shows that the chip design consists of three elements; the heating surface, flange, and a stem. The heating surface has a 10 mm x 10 mm face with a thickness of 1 mm. The thickness provides rigidity, strength, and stock to rebuff for multiple uses. The flange has a length of 24 mm, a width of 24 mm, and a thickness of 1 mm. 4 holes of 4 mm are provided on each corner to enable the chip's bolting on the garolite block. The modification eliminates the need for external restraint in the form of a strap/shim enabling convenient high-speed imaging. The stem is 10 mm wide and 10 mm thick, with a height of 9 mm. The stem houses the three holes for thermocouples equidistant to each other at 3mm.

Figure 8 Fabricated Copper Heating Chip

Figure 8 shows the fabricated chip ready to be assembled in the setup. To ensure 1D heat transfer, the flange of the chip is covered with high-temperature resistant Kapton tape to prevent heat transfer from the flanges. This prevents heat dissipation through the transverse axis and allows heat transfer through the surface only. During the experimentation, the spacing between the measurement of thermocouples T_1, T_2, and T_3 is monitored to ensure 1D heat conduction across the copper heating chip. More information about thermocouple spacing is provided in Appendix B at the end of the report.

5.2 Housing

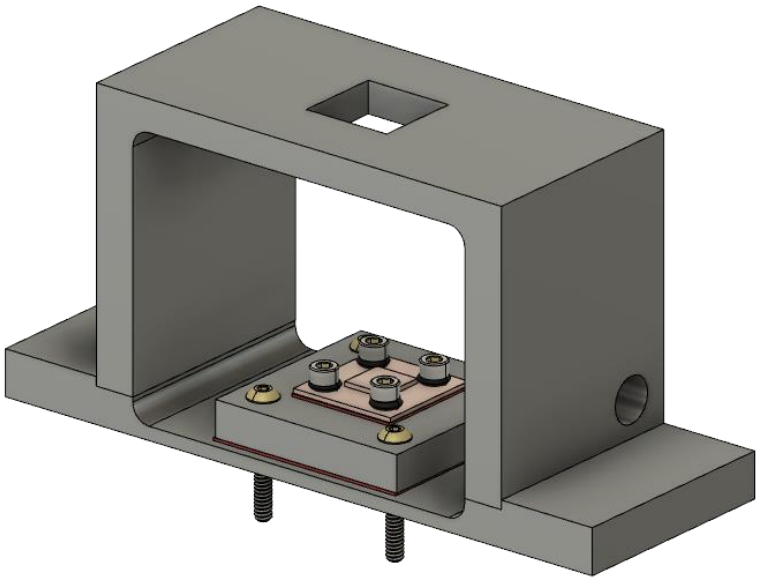

Figure 9 CAD Assembly of Housing

Figure 9, shown above, represents the assembly housing. The housing is CNC machined from Aluminum 6061 billet. The heating chip is bolted on a garolite block, further bolted on the housing's bottom section. Leaks are prevented using silicon gaskets and rubber o-rings. The vapor

is generated from the boiling vents from the top through the venting hole, thus maintaining atmospheric pressure inside the assembly. Constant liquid supply in the housing is achieved through a hole positioned on the housing's left facet. Finally, the housing is sealed from the front and backside using thick glass slides and clamped between aluminum plates.

5.3 Assembly

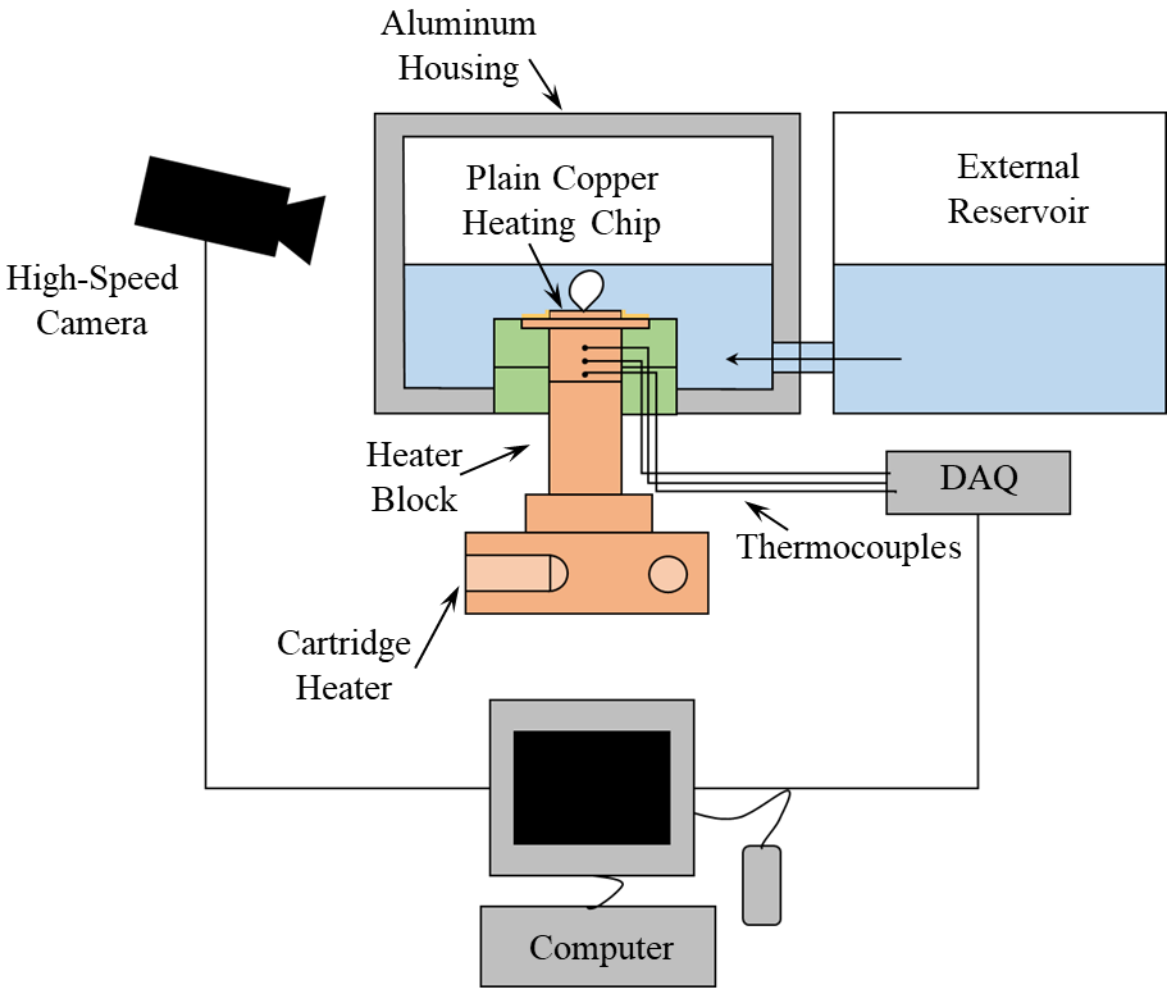

Figure 10 Pool Boiling Setup Schematic

Figure 10 shows the schematic diagram of the whole assembly. The aluminum housing is connected with an external reservoir through a transparent flexible tube and rested on a wooden

platform. The external reservoir works on the principle of the siphon and provides a constant height throughout the experiment. Make-up water can be added to the external reservoir on an as-needed basis. The volume of the reservoir provides enough factor of safety to accommodate for evaporation losses. Calculations of the volume balance can be found in the appendix section.

Thereafter, the thermocouples are inserted into the copper heating chip, and distilled water is filled to the desired height. The primary source of heat in the setup is the bunch of four cartridge heaters inserted into the heater block. The heater block is lifted using a scissor lift and brought in contact with the copper heating chip.

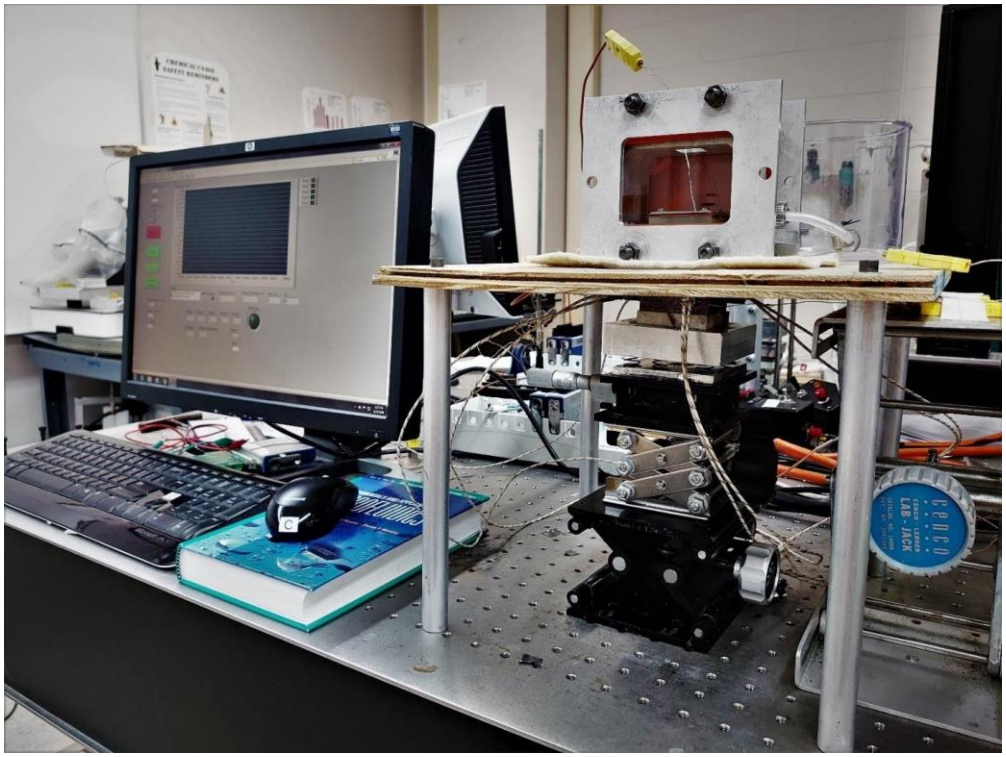

Figure 11 Actual Pool Boiling Setup

Figure 11 shows the actual pool boiling setup. In conjunction with the thermocouples inserted into the copper heating chip, another thermocouple is inserted into the liquid bulk to monitor its temperature. The data logging is explained in the upcoming section.

5.4 Data Acquisition:

To calculate heat flux and monitor pool conditions, monitoring, and recording temperature from various locations becomes crucial. Temperatures are measured from 5 distinct locations on the setup using thermocouples, a National Instruments NI-9211 temperature module equipped with National Instruments Ni-cDAQ-9172 chassis is used.

Since the temperature at the surface of the heating chip can not be measured accurately, Fourier's 1-D conduction law is utilized to approximate the surface temperature using heat flux between two points. However, to approximate the heat flux as accurately as possible, Taylor's backward series expansion is applied. To find out the heat flux, three equally spaced temperature readings are recorded from the heater block. As seen in Figure 11, three thermocouples are in contact with the heater block to record temperature T_1, T_2, and T_3.

Now that flux is calculated using T_1, T_2, and T_3 temperatures, the surface temperature can be found using the thermocouple placed inside the chip. Lastly, T_4 temperature is recorded from the liquid bulk to monitor the pool's condition, and hence it is dipped inside the pool from the top, as seen in figure 11.

5.5 Morphological Study

Since the research focuses on studying the influence of liquid height, other parameters need to be regulated. Thus, surface roughness and contact angle play a crucial role in the regulation of these parameters. In the following sections, more information is provided on the processes to measure the respective data.

5.5.1 Surface Roughness

Figure 12 Keyence VK9700 Laser Microscope

Figure 12 shows the laser confocal microscope used to observe the surface roughness of the heating chip. The model name of the laser confocal microscope is modeled VK9700, and it is manufactured by Keyence. The step by step focus allows scanning several layers of the substrate surface to measure and analyze surface morphology like surface roughness. To increase the accuracy of readings, roughness from five different locations are checked. For a heating chip surface to be characterized as smooth, a roughness of 2 microns to 3 microns is maintained.

5.5.2 Contact Angle

Figure 13 VCA Optima Optical Goniometer

The contact angle is a crucial factor in defining any solid's behavior when interacting with a liquid. The contact angle can be defined as the angle made by the liquid with the surface. It helps in determining the wettability of a surface. A surface with a contact angle less than 90° is called a hydrophilic surface, and a surface with a contact angle greater than 90° is called a hydrophobic surface. For a plain copper chip, a contact angle in a range of 70^{o} to 80^{o} is maintained.

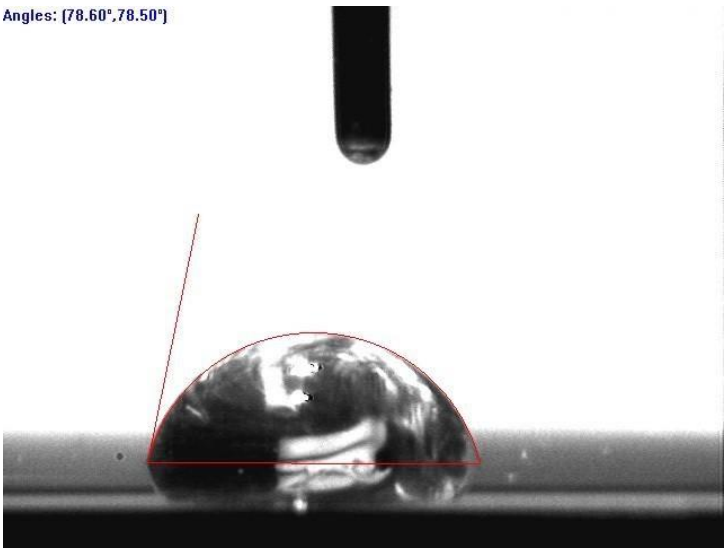

Figure 14 Contact Angle at Heating Surface

Measurement of contact angle along the surface of the heating chip is done using the VCA Optima optical goniometer's help. The goniometer is equipped with a camera that can magnify the droplet by 35 times to project a clear image of the droplet interface to measure the contact angle.

5.6 Experimental Procedure

To achieve reliable and repeatable results, a standard operating procedure is required. The procedure helps in guiding through processes and tracking changes and sources of errors. The standard operating procedure for conducting the experiments is described below.

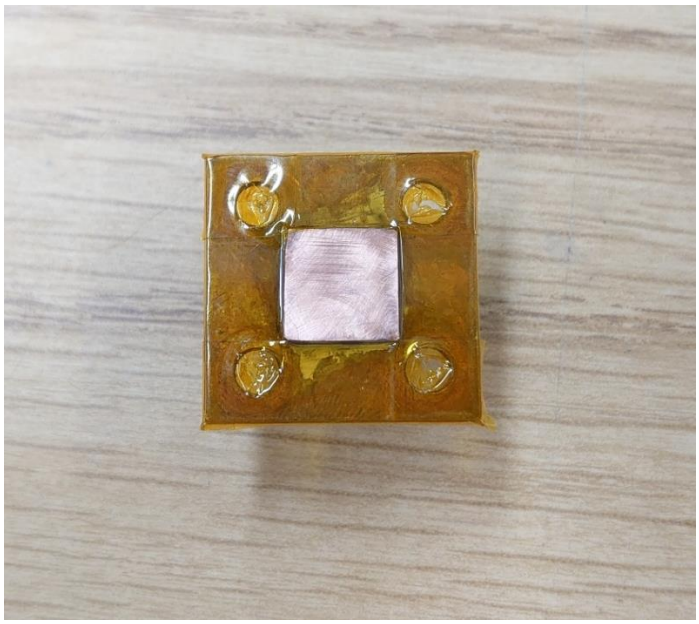

Figure 15 Copper Heating with Kaptan Tape

First, the surface of the heating chip needs to be cleaned off any impurities or irregularities. To clean the surface, the surface is rinsed with isopropyl alcohol. Once the surface is prepared, the heating chip is scanned under a laser microscope and a goniometer to measure the surface roughness and the contact angle. However, if the measured surface roughness is beyond or under

the surface roughness requirements, the heating chip's surface is hand buffed using sandpaper until the desired surface roughness is not achieved.

Once the surface's quality is under control, the chip is marked with Kapton tape to allow the conduction of heat from just a 10 mm x 10 mm surface area. Figure 15 shows a plain heating surface prepped and ready to be used for the experiment.

Figure 16 Actual Pool Boiling Setup

After preparing the chip, the chip is assembled inside the garolite block with gaskets in between, and a retaining plate bolted from the top into the base of the housing below. Following the housing assembly, glass plates are mounted on the sides with gaskets silicon rubber gaskets sandwiched in

between to prevent leaking. The complete assembled housing is placed upon a wooden platform, and the heater block is lifted from underneath to contact the heating chip, as shown in figure 16. Eventually, a beaker is connected to the housing through a flexible hose to supply make-up water. Lastly, the beaker is filled with adequate water to reach a predefined height. In the case of reaching CHF, a safety knob is turned counterclockwise to bring the heater block down and prevent further damage to the heating chip. Consequently, the voltage source is reduced to 0 V and turned off to prevent the heater block's further heating.

Once the setup is complete, all the electrical connections are connected, and gradually, power is supplied to the heating chip. Subsequently, the liquid pool in the housing reaches saturation temperature, and eventually, cavities nucleate, and boiling is initiated. At a given power, the system is allowed to reach a steady-state (the variation in temperature remains within ± 0.1°C of the mean), and after that, temperatures are recorded before increasing the power slightly again by 3 W/cm^2. This process is repeated until CHF is reached. When CHF is reached, the voltage is reduced to zero to cut off the heat supply and avoid overheating the copper heating chip. The setup is cooled down, dissembled, and all the surfaces are wiped dry using isopropyl alcohol.

6.0 Output

6.1 Data Acquisition

Temperatures are recorded at four different locations to identify the state of boiling during an experiment. The data acquisition system comprises of following components:

1. Thermocouple
2. Analog temperature module
3. Logging Device

Temperature is recorded using K type thermocouple manufactured by Omega. The thermocouples generate an analog signal which is conditioned by the National Instrument NI-9211analogue temperature module. The module is mounted on the Ni-cDAQ-9172 chassis. Together with the module and chassis, LabView provides the software to monitor and record the temperature on to the computer.

Out of the four thermocouples used to monitor the experiment, three thermocouples are used to monitor the copper heating chip's temperature as discussed in the previous section, and the fourth thermocouple is used to measure the temperature of liquid bulk. The output from these thermocouples can be monitored on LabView and stored on the Computer for further calculations.

6.2 Heat Transfer Calculations

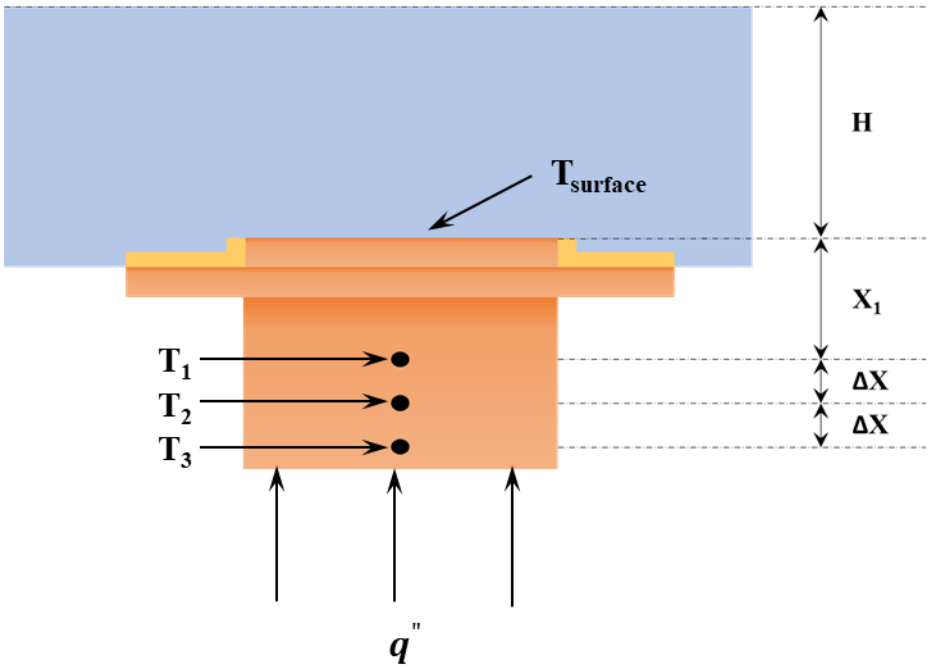

Figure 17 Copper Heating Chip Schematic

Figure 17 shows the schematic of the heat supply to the plain copper heating chip. The heat flux, q" is the heat per unit area conducting from the bottom of the heating chip to the heating chip's surface. Fourier's 1-D conduction equation can calculate the heat flux. The equation is given by:

$$q^{"} = -k_{Cu}\frac{dT}{dx} \quad (1)$$

In the above equation, dT/dx is the temperature gradient in the heating chip's stem. The temperature gradient can be found out using Taylor's backward series expansion, which can be given as follows:

$$\frac{dT}{dx} = \frac{3T_1 - 4T_2 + T_3}{2\Delta x} \quad (2)$$

Considering Fourier's 1D conduction law, the temperature on the heating chip surface can be calculated as follows:

$$T_{surface} = T_1 - q^{"}\left(\frac{x_1}{k_{Cu}}\right) \quad (3)$$

Using the above temperatures, we can find the HTC, as follows:

$$h = \frac{q^{"}}{T_{surface} - T_{saturation}} \quad (4)$$

6.3 Error Analysis

While experiments are conducted with the utmost care and meticulous approach, some error sources still affect the data and the subsequent results. The origins of errors can be classified into two types of errors.

1. Bias Error:

- Biases in measurement device which result in measurements that differ significantly from the actual value result in bias error
- Bias error results in a smaller or larger measurement than the actual value but not both
- Bias errors can be corrected through calibration

2. Precision Error:

- The ability of an instrument to keep an agreement is between repeated measurements is called precision error
- Precision error is a result of scattered measurements
- A precision error cannot be eliminated through calibration

The significant error sources for this research can be sourced to copper's purity used to manufacture heating chip and heater block, thermocouples, and Vernier caliper. Some of the errors can be mitigated through calibration, and hence thermocouples are calibrated, and the adjusted values are fed into the data acquisition system. However, the error in the results can be found as follows:

The total error can be found as follows:

$$U_{q"} = \sqrt{B_{q"}^2 + P_{q"}^2} \tag{5}$$

Where $B_{q"}$ and $P_{q"}$ are the bias and precision errors, respectively.

The general equation to find an error in a system can be found using the following expression.

$$U_x = \sqrt{\sum_{i=1}^{n} \frac{\delta q}{\delta U_i} U_i^2} \tag{6}$$

Hence, upon plugging the various uncertainties into the above equation, we can find an equation suitable for our purpose. The uncertainties surrounding this research's calculations are the thermal conductivity coefficient of copper, T1, T2, and T3 thermocouple temperatures and the distance measured between those thermocouples Δx.

These variables' uncertainties can be found by finding the standard deviation of each value from the mean and then multiplying them with the actual value. The uncertainty analysis has been conducted with 95% confidence assuming the data to be represented with a normal distribution curve.

Plugging the variables mentioned above into the equation (6), total bias uncertainty can be expressed as follows:

$$U_{q^{''}} = \sqrt{\left(\frac{\partial q^{"}}{\partial K_{Cu}}\right)^2 \left(U_{K_{Cu}}\right)^2 + \left(\frac{\partial q^{"}}{\partial x}\right)^2 (U_x)^2 + \left(\frac{\partial q^{"}}{\partial T_1}\right)^2 \left(U_{T_1}\right)^2 + \left(\frac{\partial q^{"}}{\partial T_2}\right)^2 + \left(U_{T_2}\right)^2 \left(\frac{\partial q^{"}}{\partial T_3}\right)^2 \left(U_{T_3}\right)^2} \quad (7)$$

Equation (7) can be modified to be expressed in terms of $q^{"}$ as following:

$$\frac{Uq^{"}}{q^{"}} \sqrt{\frac{\left(\frac{\partial q^{"}}{\partial K_{Cu}}\right)^2 \left(U_{K_{Cu}}\right)^2 + \left(\frac{\partial q^{"}}{\partial x}\right)^2 (U_x)^2 + \left(\frac{\partial q^{"}}{\partial T_1}\right)^2 \left(U_{T_1}\right)^2 + \left(\frac{\partial q^{"}}{\partial T_2}\right)^2 + \left(U_{T_2}\right)^2 \left(\frac{\partial q^{"}}{\partial T_3}\right)^2 \left(U_{T_3}\right)^2}{q^{"2}}} \quad (8)$$

Differentiating the sensitivity coefficients can be calculated as follows:

Assuming, $\alpha = 3T_1 - 4T_2 + T_3$ (9)

$$\left(\frac{\partial q^{"}}{\partial K_{Cu}}\right)^2 = \left(\frac{q^{"}}{kcu}\right)^2 \quad (10)$$

$$\left(\frac{\partial q^{"}}{\partial x}\right) = \frac{\left(-q^{"}\right)^2}{\Delta x} \quad (11)$$

$$\left(\frac{\partial q^{"}}{\partial T_1}\right)^2 = \frac{9q^{"2}}{\alpha^2} \quad (12)$$

$$\left(\frac{\partial q^{"}}{\partial T_2}\right)^2 = \frac{16q^{"2}}{\alpha^2} \quad (13)$$

$$\left(\frac{\partial q^{"}}{\partial T_3}\right)^2 = \frac{q^{"2}}{\alpha^2} \quad (14)$$

Upon substituting equations (9), (10), (11), (12), (13), (14) into equation (8), we get the final expression as follows:

$$\frac{Uq^{"}}{q^{"}} = \sqrt{\frac{\left(U_{K_{Cu}}\right)^2}{K_{Cu}^2} + \frac{(U_x)^2}{\Delta x^2} + \frac{9\left(U_{T_1}\right)^2}{\alpha^2} + \frac{9\left(U_{T_2}\right)^2}{\alpha^2} + \frac{9\left(U_{T_3}\right)^2}{\alpha^2}} \quad (15)$$

Equation (15) provides the general expression to calculate the bias error for a given data point of a pool boiling experiment. Table 1 lists the uncertainty associated with each parameter.

Table 1 Bias Uncertainty

Parameter	**Value**	**Unit**	**Biased Uncertainty**	**% Uncertainty**
$\mathbf{K_{Cu}}$	391.000	W/m°C	9.000	2.301%
Δx	3.000	mm	0.010	0.333%
$\mathbf{T_1}$	Varies with temperature	°C	0.065	Varies with temperature
$\mathbf{T_2}$	Varies with temperature	°C	0.065	Varies with temperature
$\mathbf{T_3}$	Varies with temperature	°C	0.069	Varies with temperature

The precision uncertainty can be calculated similarly using equation (15). However, the uncertainties of thermocouple T_1, T_2, and T_3 are plugged in from thermocouple calibration.

Total uncertainty can be calculated using equation (5).

Finally, the error percentage can be calculated as follows

$$E\% = \frac{U_{q''}}{q''} x\ 100\% \quad (16)$$

Figure 18 shows the error across the heat flux range for the pool boiling experiment conducted at 15mm liquid height.

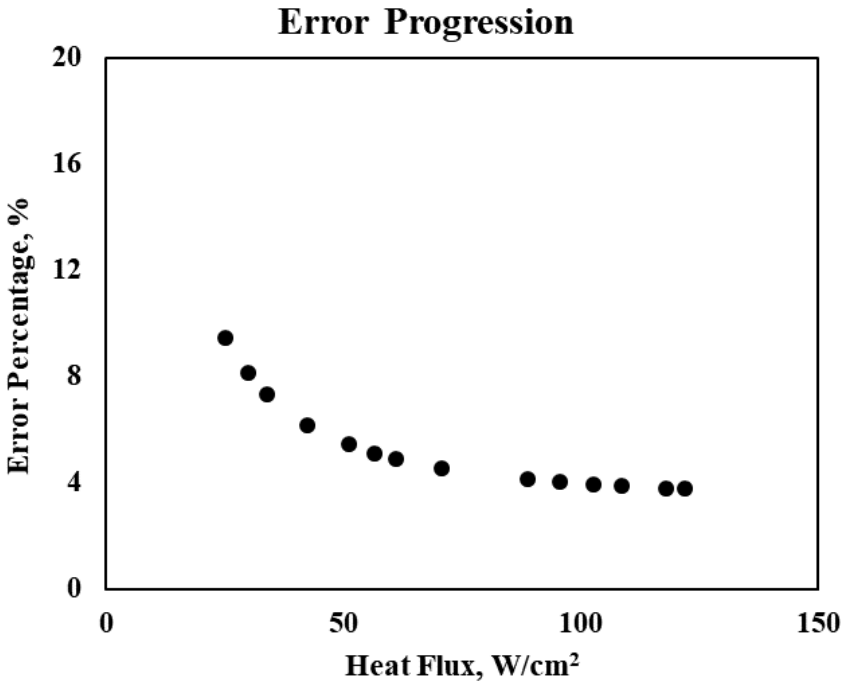

Figure 18 Error Progression

It can be seen from the figure that while at lower heat fluxes, the error is about 10%, but it starts to decrease as heat flux is increasing. Near CHF, the error creeps down to about 4% of the total heat flux. The proportionality of error concerning the heat flux can be attributed to reducing error at higher heat fluxes. The uncertainty analysis of the remainder experiments shows similar results. Therefore, to avoid clutter, error bars only for one data set is shown. Further analysis of the error is presented in the upcoming result section.

7.0 Results

This section discusses the results obtained from the experiments performed in the previous sections. All the tests performed in this study were performed at atmospheric pressure using distilled water as the boiling medium over a copper heating chip.

7.1 Comparing Critical Heat Flux and Wall Superheat

Figure 20 shows the pool boiling curve obtained after compiling results from all the pool boiling experiments conducted over the plain copper heating chip at different liquid heights. The experiments were carried out in the carefully designed setup as described earlier. The horizontal axis shown in the plot represents the wall superheat, and the vertical axis represents heat flux. The wall superheat is the temperature difference between the heating chip's surface temperature and the water's saturation temperature. The unit of wall superheat is °C, and the unit for heat flux is W/cm^2.

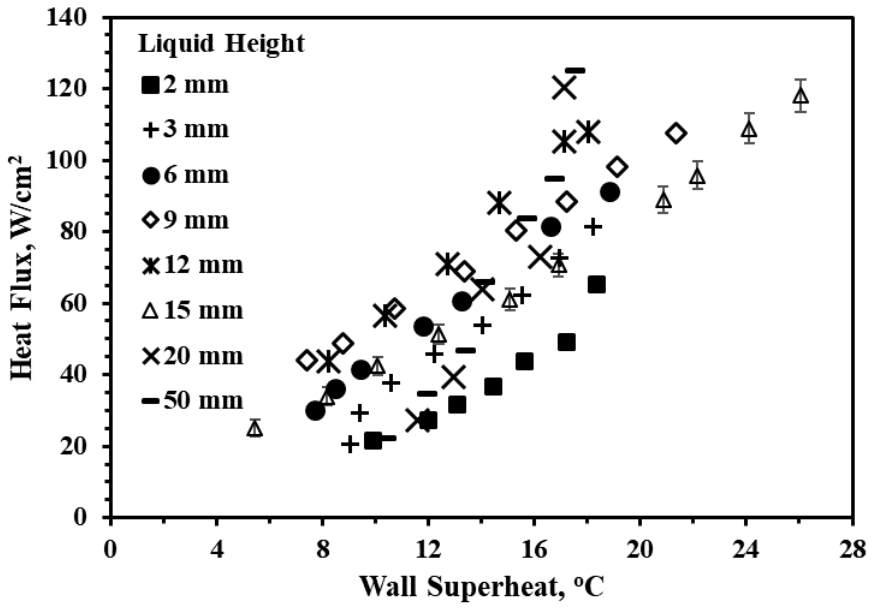

Figure 19 Experimental Pool Boiling Curve over a Plain Copper Chip

As seen in the pool boiling curve shown above in figure 19, are the cumulative results of experiments conducted at the liquid height of 2 mm, 3 mm, 6 mm, 9 mm, 12 mm, 15 mm, 20 mm, and 50 mm. The pool boiling experiment results at 50 mm liquid height comparable to that observed by Jaikumar and Kandlikar over a plain copper chip with CHF around 125 W/cm^2 and a wall superheat of about 18°C. Reducing the liquid height to 20 mm, the pool boiling curve shows similar performance with CHF observed at around 122W/cm^2 and wall superheat of about 16°C. Upon further reducing the liquid height to 12 mm and 6 mm, it can be observed that the CHF reduced to around 105 W/cm^2 and 90 W/cm^2 with a wall superheat of around 17 °C and 18°C, respectively. Similarly, when we look at the pool boiling curve for 3 mm and 2 mm liquid height, the CHF further reduces to 80W/cm^2 with a wall superheat of around 17 °C and 60W/cm^2 a wall superheat of around 18 °C, respectively.

However, when the graph is split into two imaginary regions, i.e., a low heat flux region below 60W/cm^2 and a high heat flux region above 60W/cm^2, it can be seen that in the low heat flux-region, for similar wall superheats, lower liquid heights perform better than higher liquid heights. However, the performance of higher liquid height improves at higher heat fluxes. The pool boiling curve for 2mm proved to be an exception as it performed poorly across both the regions. The improvement pattern can be noted as supplied heat flux increases, and the boiling performance gets better with increasing liquid height.

Figure 20 reduces the results from figure 19 and shows the pool boiling curve for experiments conducted at 2 mm, 6 mm, 12 mm, and 50 mm liquid height. Figure 20 shows the wall superheat observed on the horizontal axis for a given heat flux on the vertical axis.

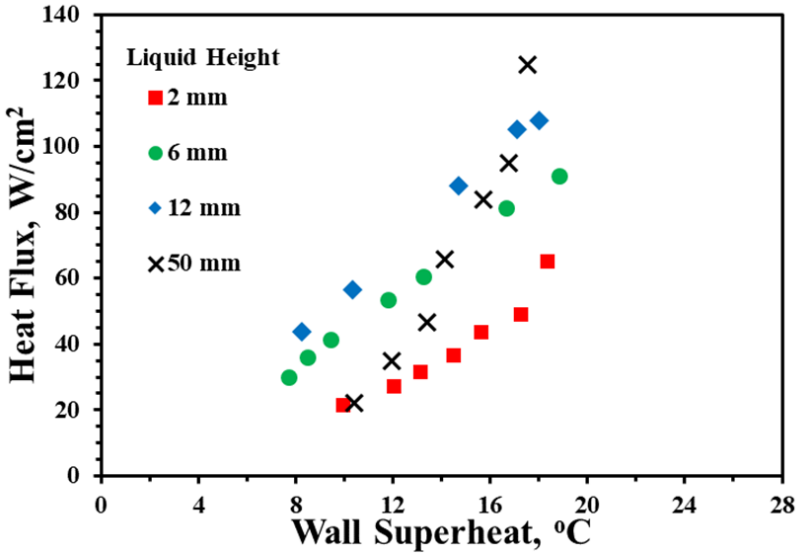

Figure 20 Observations from pool boiling study conducted at different liquid heights

It can be noted from figure 20 that the pool boiling experiment conducted at 50 mm shows similar performance to pool boiling experiments conducted by other researchers over a plain copper heating surface.

Moreover, it can be observed that with a reduction in liquid height, the CHF reduces too. Furthermore, it can be observed that at low liquid height, the heat transfer coefficient is larger compared to the pool boiling experiment conducted at a liquid height of 50 mm. The pool boiling experiment conducted at 2 mm liquid height performs the least because of unstable boiling. This instability can be attributed to the short liquid height in comparison with the departing bubble diameter.

Figure 21, shown below, reduces the data from figure 19 and plots CHF in W/cm^2 as a liquid height function in mm. Generally, it can be seen that CHF increases until the liquid height is 20 mm. However, it can be observed that beyond 20 mm of liquid height, there is no further enhancement in CHF. Furthermore, the reduction in CHF is most severe at 2 mm liquid height.

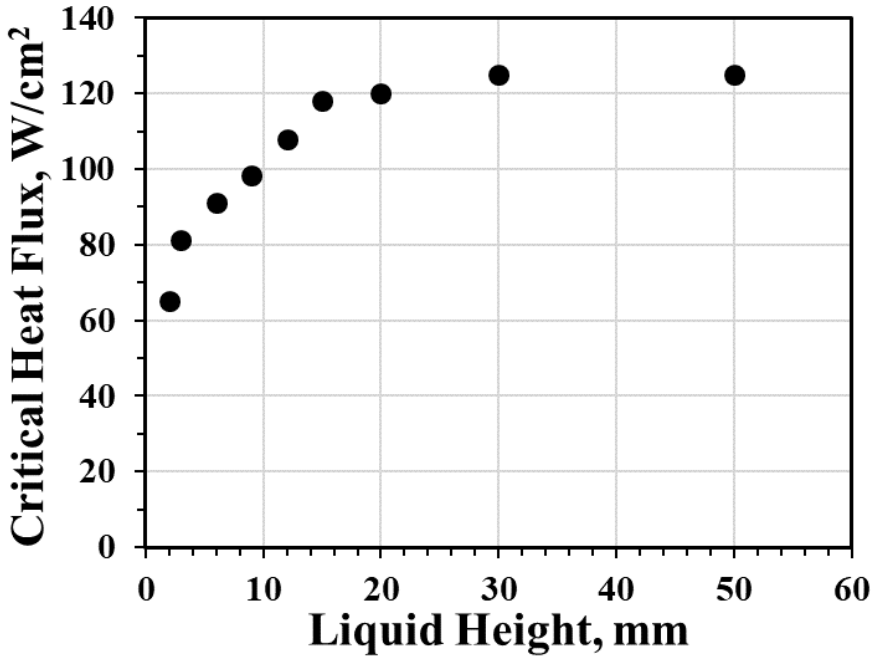

Figure 21 CHF as a function of liquid height

Hence, to summarize, it can be asserted from the preliminary experiments that there is a significant impact of bulk liquid height on pool boiling performance. While the pool boiling curve for 50mm and 20mm pool height shows an elevated CHF, performing the pool boiling experiments shows a varying liquid trend. The sections below enunciate the performance parity.

7.2 Comparing Heat Transfer Coefficient

To understand the influence of liquid height on Heat Transfer Coefficient, Figure 22, as shown below, is generated. The graph compares the heat transfer coefficient for similar heat fluxes at different liquid heights. The liquid height defines the horizontal axis, and the unit of representation is mm. The vertical axis represents the heat transfer coefficient in kW/m^2K for the heat flux of $25W/cm^2$, $45W/cm^{2,}$ and $65W/cm^2$. The heat transfer coefficient is calculated as described in the earlier section. Data points from Nishikawa's research at a heat flux of 6.49 W/cm2 are reconstructed to aid understanding.

When observing from higher heat flux to lower heat flux, it can be seen from the plot made for 65 W/cm^2 heat flux that at 2 mm, the corresponding heat transfer coefficient is about 35 kW/m^{2}K. The heat transfer coefficient increases to a peak at about 55 kW/m^{2}K at a liquid height of 12mm. Thereafter, the heat transfer coefficient plateaus around 47 kW/m^{2}K for a liquid height of 20mm and 30mm. The plots for 45W/cm^2 and 25W/cm^2 show a similar heat transfer coefficient pattern. Consequently, it can be observed that all the three contours peak at 12mm liquid height. Its difference in performance can be linked with the difference in bubble movement, as observed during the experiment.

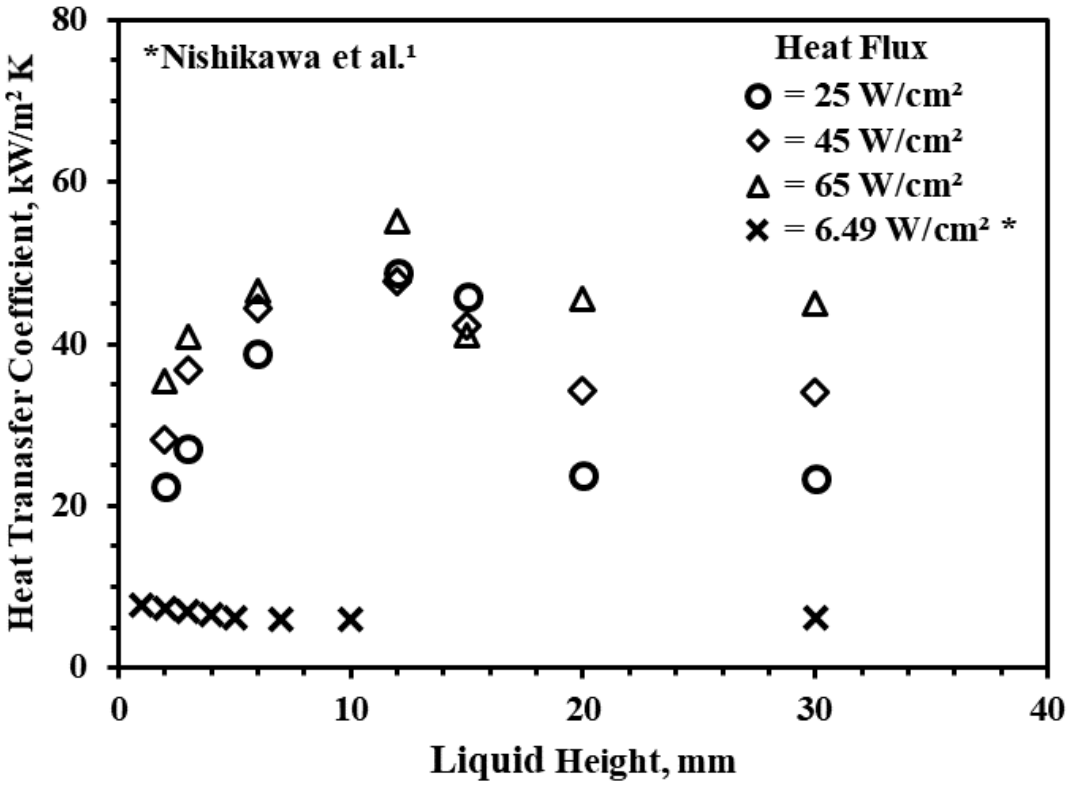

Figure 22 Heat Transfer Coefficient Comparison

On the other hand, the contour from Nishikawa's data shows different behavior. The heat transfer coefficient calculated for the aforementioned author's data point is calculated at a heat flux of 6.49 W/cm^2. Overall, it is seen that the heat transfer coefficient increases with decreasing liquid height.

Also, significant improvement in the heat transfer coefficient can be observed below the liquid height of 5mm. The maximum heat transfer coefficient observed was around 8kW/ m^2K at 1mm liquid height. However, a significant point of consideration for the plot is the low supplied heat flux. The authors also report that the bubble generation was discrete and did not contribute significantly to the heat transfer process.

Hence, to summarize, it can be concluded that while 12mm liquid is provided with the best heat transfer coefficient across all the liquid heights. The difference in heat transfer performance is linked with the bubble movement observed during the pool boiling experiments. The following sections will discuss the bubble movement in detail.

7.3 High-Speed Visualization

The previous sections and visual observations stimulate high imaging to understand the bubble movement for a clearer understanding of the underlying mechanism. This section will suggest the underlying mechanism based on evidence as observed from high-speed images.

7.3.1 Actual High-Speed Images

Using a high-speed camera, nucleating bubbles were recorded at a high frame rate and analyzed on a frame by frame sequence to evaluate the movement. Based on the recorded video, a vapor bubble in the pool boiling experiment goes through different stages. The stages are bubble nucleation, bubble growth, bubble coalescence, bubble detachment, and bubble exit. These six stages are represented by the frame captured and shown below. Evaluating the differences between these sequences provide the reason for such a difference in the performance.

Figure 26 below describes the six stages of a vapor bubble in a pool boiling at 20mm liquid height. Due to optical limitations, the liquid-gas interface is not visible in the frame sequence. However, the movement and departure of the bubble can be well observed from the available point of view.

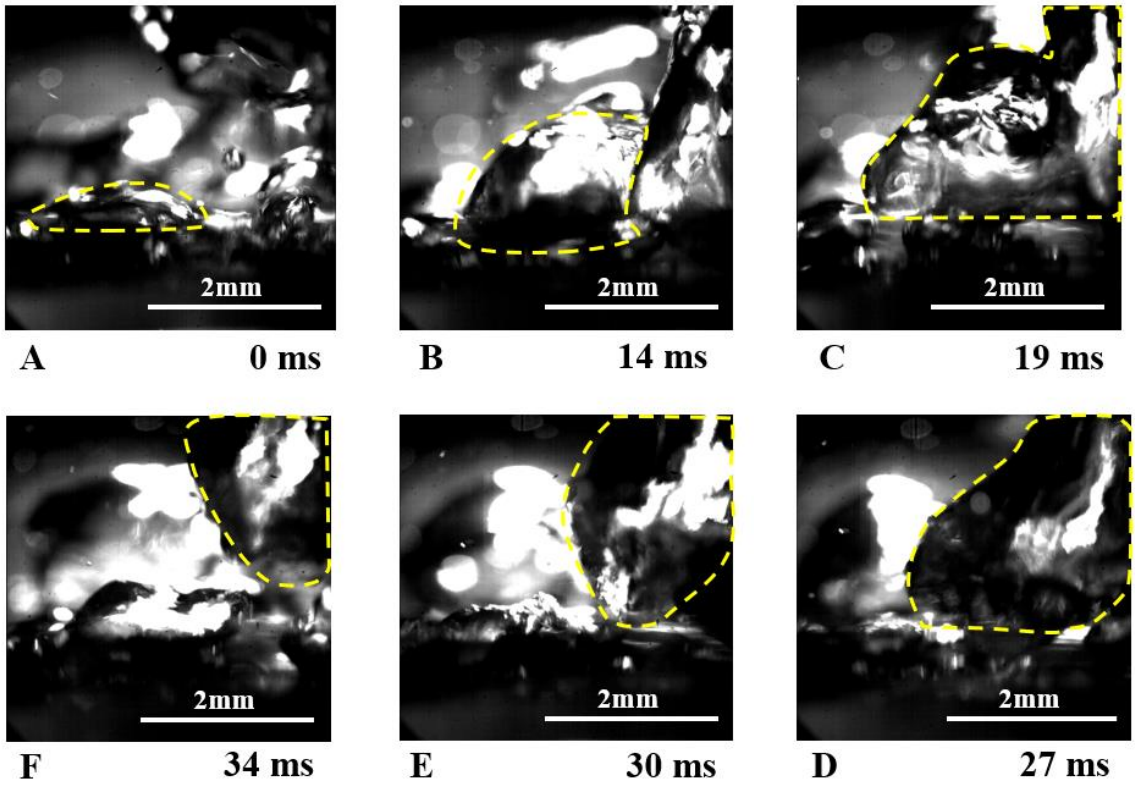

Figure 23 High-speed images at 20 mm liquid height

Figure 23(A) shows the nucleation of a tiny bubble on top of the plain copper heating surface. In the next 14 milliseconds, the bubble grows and almost comes in contact with the adjacent bubble, as shown in Figure 23(B). In the next five milliseconds, the bubble coalesces with the adjacent vapor bubble and gains volume, as seen in Figure 23(C). Figure 23(D) shows that the coalesced slug enlarges over the next eight milliseconds and tries to reach the liquid height. Subsequently, in the next three milliseconds, as seen in Figure 23(E), the bubble detaches itself from the surface and rises to the liquid-gas interface. Finally, after 34 milliseconds from its nucleation, the bubbles lift from the bottom and vents into the surface, as seen in Figure 23(F).

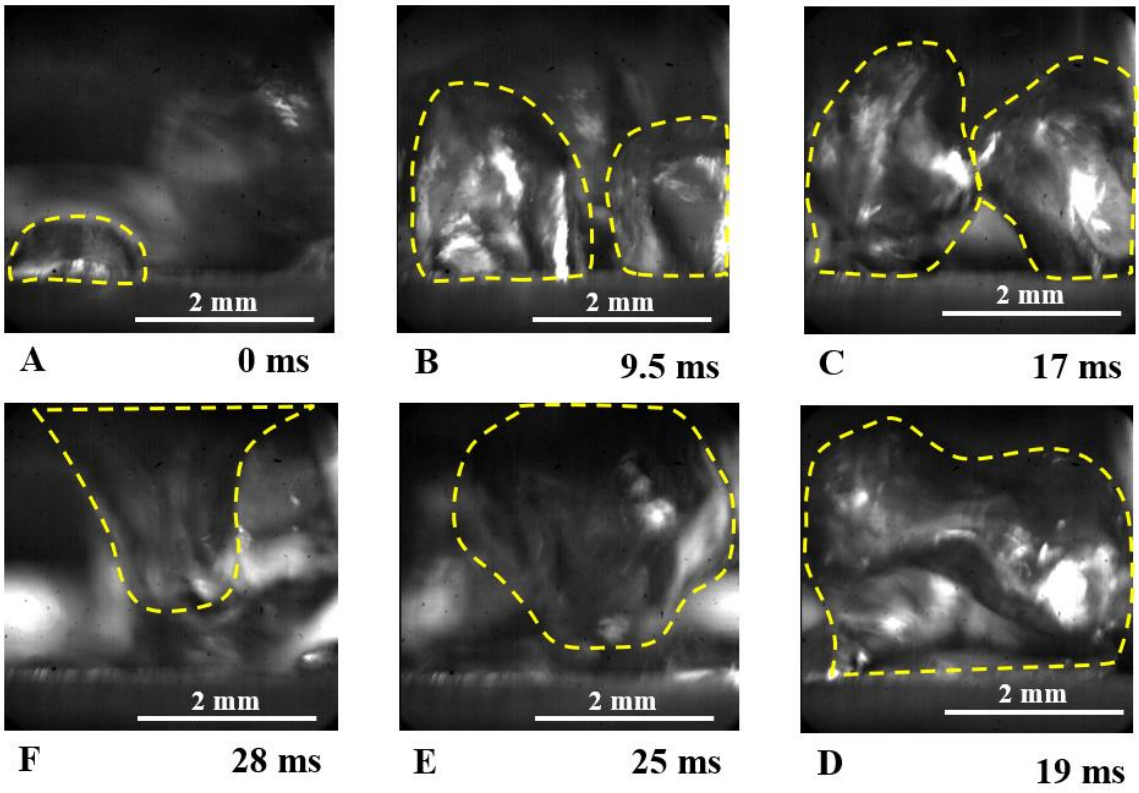

Figure 24 High-speed images at 12 mm liquid height

Figure 24 shows the six stages of a vapor bubble in a pool boiling at 12mm liquid height. Due to optical limitation, neither the heating surface nor the liquid-gas interface is visible. However, the boundaries mentioned above near the top and bottom edges of the frame, and hence fair analysis can be made on the vapor bubble's movement. Figure 24(A) shows the nucleation of a tiny bubble on top of the plain copper heating surface. In the next 9.5 milliseconds, the bubble grows in size, as shown in Figure 24(B). In Figure 24(C), it can be observed that the vapor comes in contact with the adjacent vapor bubble. After almost 19 milliseconds post the nucleation, the vapor bubble coalesces to the adjacent bubble and forms an enormous slug. As shown in Figure 24(D). Subsequently, in the next six milliseconds, as seen in Figure 24(E), the slug detaches from the surface and rises towards the liquid-gas interface. Eventually, after 28 milliseconds, the bubbles vents into the atmosphere, as observed in Figure 24(F).

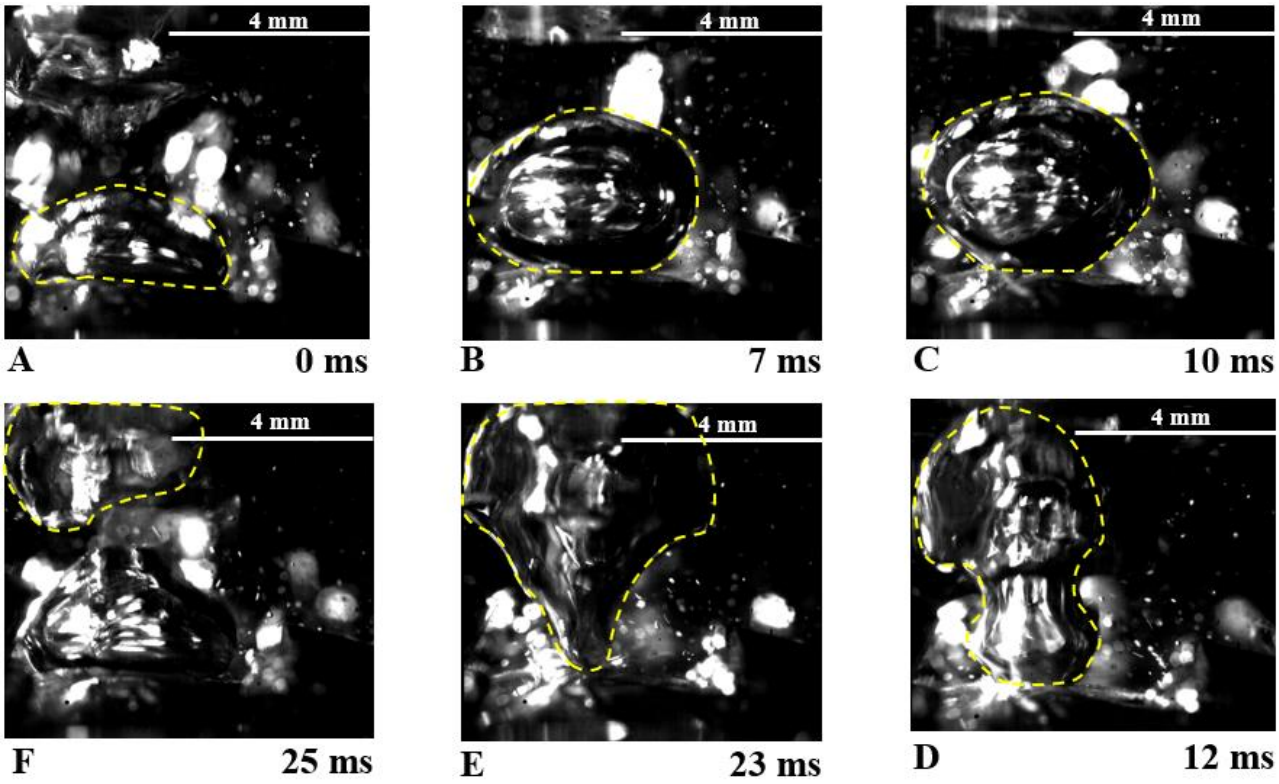

Figure 25 High-speed images at 6 mm liquid height

Figure 25 shows the six stages of a vapor bubble in a pool boiling at 6mm liquid height. Figure 25(A) shows the nucleation of a tiny bubble on top of the plain copper heating surface marked with a yellow line. In the next seven milliseconds, the bubble grows, as shown in Figure 25(B). In the next three milliseconds, the bubble further grows in size, as seen in Figure 25(C). In the next couple of milliseconds, the bubble coalesces with another bubble, as seen in Figure 25(D). In the next 11 milliseconds, Figure 25(E) shows that the bubble grows further and simultaneously detaches from the plain copper heating surface. In the last sequence, Figure 25(F), it can be seen that the bubble leaves the surface and vents into the atmosphere leaving behind ample volume for water to rewet the surface.

Figure 26 shows the six stages of a vapor bubble in a pool boiling at 3mm liquid height. Figure 26(A) shows the nucleation of two tiny bubbles on top of the plain copper heating surface. In the next two milliseconds, the bubble grows and comes in contact with each other, as shown in Figure 26(B). In the next three milliseconds, the bubble coalesces with the adjacent bubble while almost growing to the size where its size almost becomes equal to the liquid height as seen by Figure 26(C). Figure 26(D) shows a giant slug-like vapor bubble formating upon the heating surface as seen previously with 2 mm liquid height in the next couple of seconds.

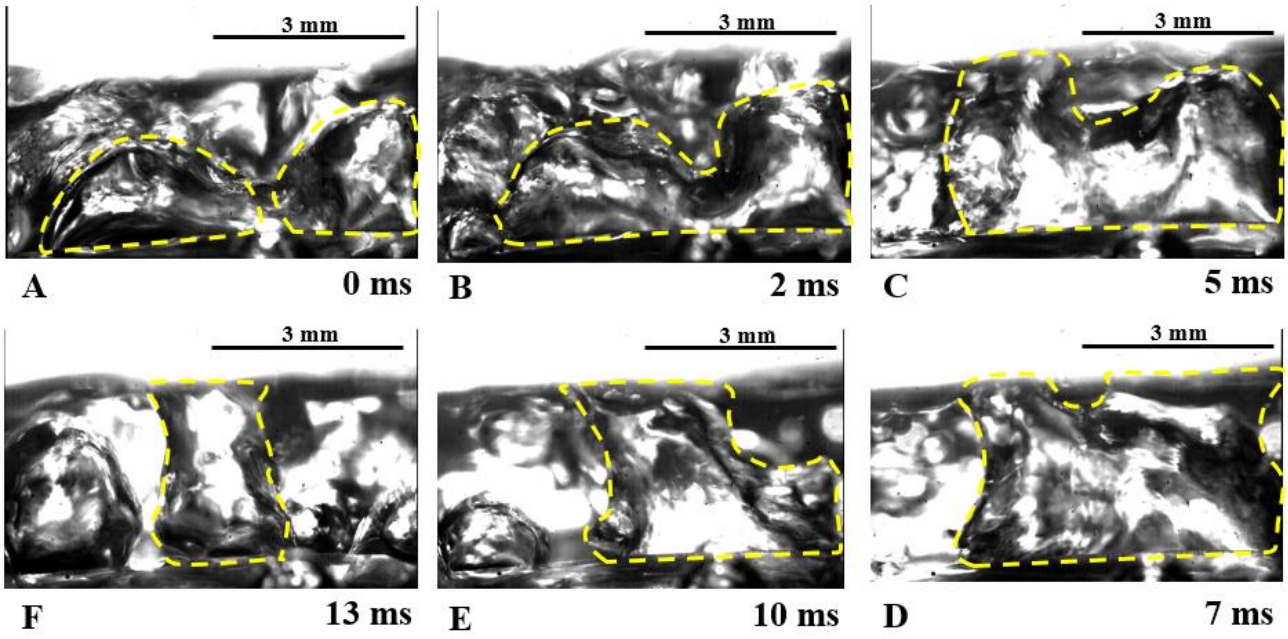

Figure 26 High-speed images at 3 mm liquid height

Subsequently, Figure 26 (E) shows that in 10 milliseconds from the nucleation, the bubble starts venting into the atmosphere while still unable to detach itself from the surface. After 13 milliseconds from the nucleation, the bubble is squeezed into the atmosphere by adjacent bubbles, as shown in figure 26 (F).

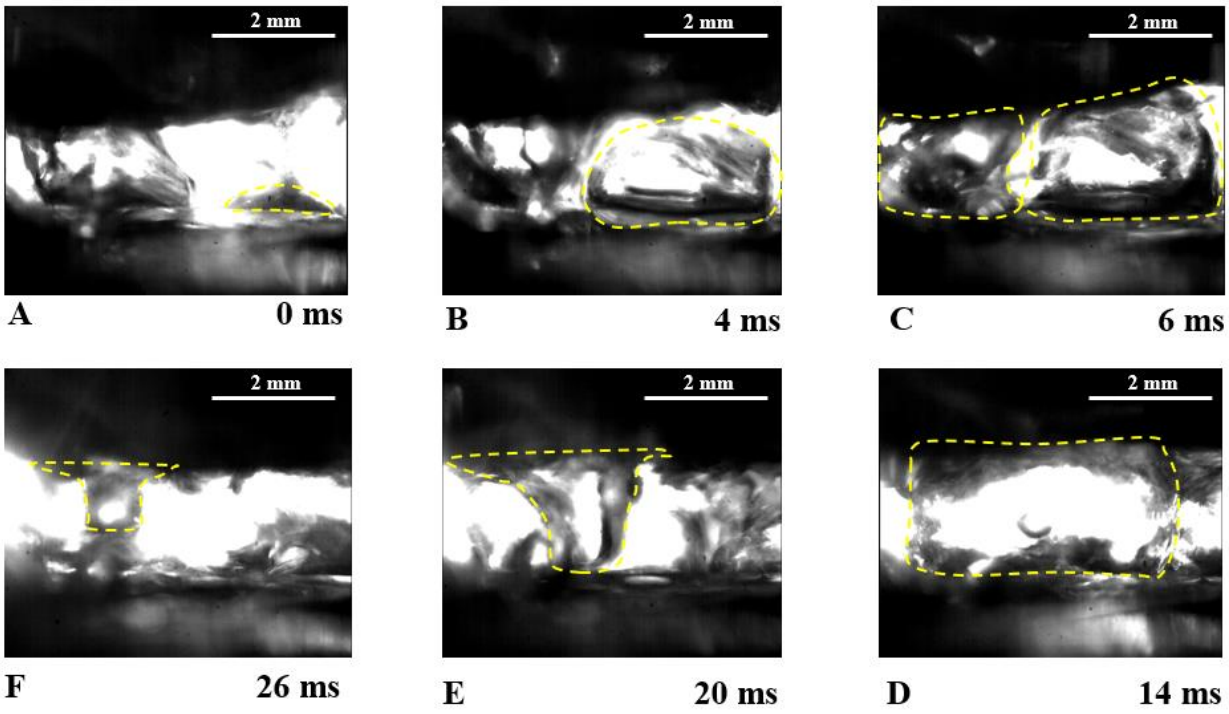

Figure 27 High-speed images at 2 mm liquid height

Figure 21 shows the six stages of a vapor bubble in a pool boiling at 2mm liquid height. Figure 21(A) shows the nucleation of a tiny bubble on top of the plain copper heating surface. In the next four milliseconds, the bubble grows, as shown in Figure 21(B). In the next couple of milliseconds, the bubble coalesces with the adjacent bubble while almost growing to the size where its size almost becomes equal to the liquid height as seen by Figure 27(C). Figure 27(D) shows the formation of a giant slug-like vapor bubble forming a dry patch atop the heating surface in a further eight milliseconds.

Moreover, this bubble prevents the rewetting of the surface. Subsequently, the next eight milliseconds in Figure 27(E) shows that the bubble tries to vent into the atmosphere while still unable to detach itself from the surface. Still unable to detach from the surface due to its large diameter compared to the liquid height, 26 milliseconds after the nucleation, Figure 27(F) shows that the bubble is pushed upwards by another bubble nucleating.

Thus, the high-speed images can be observed in a regular pool boiling setup, the vapor bubble has enough space to detach from the surface and travel upwards into the atmosphere. While this space allows for rewetting the surface to achieve higher heat flux, it creates greater resistance for the bubble to dump the heat. On the other hand, the lower liquid height provides lesser resistance for the vapor bubble to dump the heat into the atmosphere but hinders the rewetting mechanism resulting in reduced CHF. The following section further elaborates on these mechanisms.

7.3.2 Graphic Visualization

The frame sequence from the high-speed videos shown in the above section suggests two underlying working mechanisms. One mechanism works at liquid heights lower than 12 mm, and another one works at liquid heights higher than 12 mm. The following section describes the two mechanisms in detail.

Figure 28 shows how boiling takes place at low liquid height over a plain copper heating chip. The figure represents different stages of boiling in different subfigures. Initially, due to the low liquid height, the liquid bulk heats up quickly to saturation temperature due to natural convection.

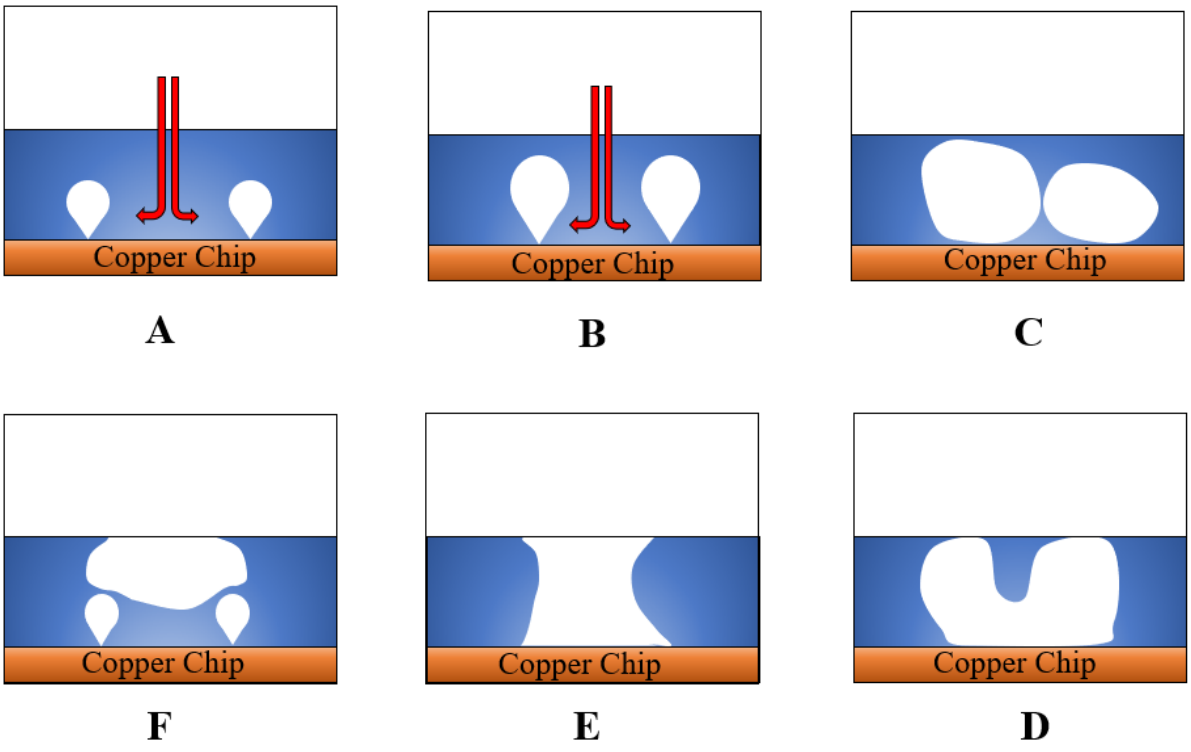

Figure 28 Graphic representation of boiling at low liquid height

Figure 28(A) shows the nucleation of the bubble over a plain copper heating chip. The arrows indicate the ample space available for the liquid to rewet the surface for an uninterrupted boiling process. Figure 28(B) shows the growth of vapor bubbles as they continue to collect more vapor. Similar to figure 28(A), the red arrows in figure 28(B) signifies available paths for the liquid to rewet. As the bubble grows further in size, adjacent bubbles come in contact with each other as they try to coalesce, as shown in figure 28(C). Eventually, they form a large coalesced slug, almost attaining the height equivalent to the liquid height shown in figure 28(D). In the frame sequence C and D, it can be noted that the bubble covers a significant region above the heating chip, and therefore liquid rewetting of the copper heating chip is affected. After that, as seen in figure 28(E), the bubbles form a trunk-like structure as they stretch from the heating surface to the liquid-gas interface as it tries to detach from the surface and vent into the atmosphere. Unable to detach, new nucleating bubbles push the bubble into the atmosphere, as seen in figure 28(F). Due to the bubble's

inability to detach from the heating surface, the liquid cannot wet the heating surface, and subsequently, the boiling process is momentarily interrupted due to lack of replenishing water. During the pool boiling experiments, this chaotic movement caused temporary spikes in the heating surface temperature. However, once these bubbles escaped and sufficient water rewet the surface, the surface temperature would return to normal. The magnitude of this phenomenon aggravates with increasing heat flux, the vapor trunk disallows water to rewet the surface, and CHF is reached. At lower heat flux, the vapor bubbles burst directly at the liquid-gas interface instead of collapsing in the subcooled liquid region as observed in higher liquid regions.

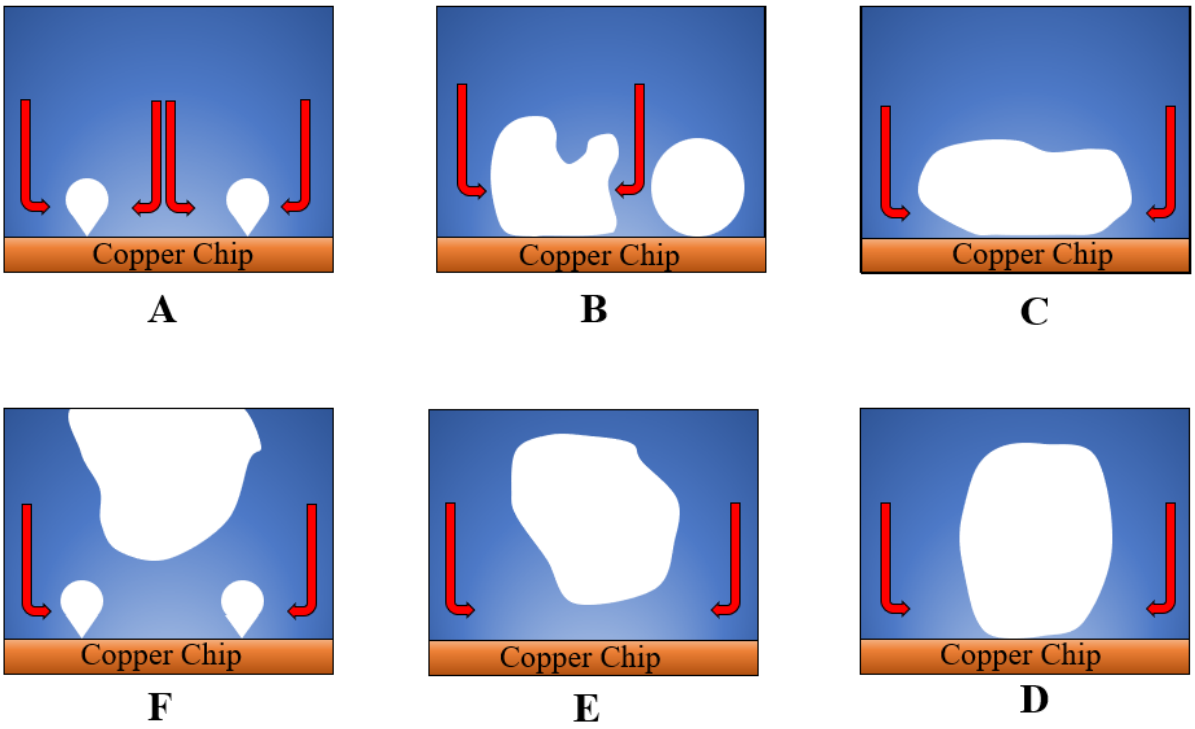

Figure 29 Graphic representation of boiling at low liquid height

Figure 29 shows the observed boiling process during the pool boiling experiments with high liquid height over a plain copper heating chip. The figure represents different stages of boiling in different subfigures. Figure 29(A) shows the nucleation of the bubble over a plain copper heating chip. The

arrows indicate the ample space available for the liquid to rewet the surface for an uninterrupted boiling process. Similar to the low liquid height boiling process, space close to the bubble is sufficient for the liquid to rewet the heating surface. Figure 29(B) shows the growth of vapor bubbles as they collect the vapor. Similar to figure 29(A), figure 29(B) shows headroom for the bubble to grow as it continues to grow.

In comparison to figure 28(B), though the bubbles grow to an equivalent size, the larger liquid height provides sufficient space for further bubble movement. As the bubble grows further in size, adjacent bubbles come in contact with each other as they try to coalesce, as shown in figure 29(C). Coalescence of vapor bubbles was observed to be similar to that of low liquid height. However, even after forming large slugs, the larger liquid height allows the bubble to grow without chaotically stretching into a trunk-like column, as shown in figure 29(D). Thereafter, as seen in figure 29(E), the vapor bubble successfully detaches itself from the heater surface and tends to rise towards the liquid-gas interface. The successful detachment allows water to wet the heating surface even at higher liquid heights. Due to the larger liquid height, the detached bubble rises to the liquid-atmosphere interface allowing for improved rewetting. Subsequently, a new vapor bubble can nucleate without interfering with the boiling process.

Due to the bubble's ability to detach from the heating surface, the liquid can continuously wet the heating, and the boiling process continues without any disruption. Compared to the boiling process observed at low liquid heights, the boiling process observed in experiments with high liquid height does not exhibit temperature spikes due to the effective removal of bubbles from the heating surface. Though at lower heat fluxes, due to the large liquid height, vapor bubbles have to travel further to dump the heat into the atmosphere, the bubble detachment from the heating surface enables rewetting of the surface. On the other hand, the low liquid height cannot provide enough

height for the bubble to detach and hence forms a foam-like layer atop the heating surface, which results in a deteriorated bubble venting process at higher heat fluxes.

The relation between liquid height and vapor bubble can be well understood if the height is non-dimensionalized. The following section elaborates on the idea further.

7.4 Non-Dimensional Height

From the previous sections, it can be realized that the relation between the pool height above the heater surface and vapor bubble diameter is one of the critical factors affecting the boiling processes because of the bubble movement across the liquid height. Figure 28, shown below, compares the heat transfer coefficient to non-dimensional height, H*.

The non-dimensional height, H* can be calculated as follows:

$$\therefore \quad H^* = \frac{Liquid\ Height,mm}{Bubble\ Diameter,mm}$$

$$\therefore \quad H^* = \frac{H}{Db} \tag{17}$$

Where,

H = liquid height corresponding to the experimental height of water during the pool boiling experiments

Db = 2.51mm (Average bubble diameter calculated from high-speed videos at a heat flux of 36W/cm^2

In the below-shown figure 28, the horizontal axis represents the non-dimensionalized height, H*. The vertical axis represents critical heat flux calculated at a heat flux of 36W/cm^2 corresponding to the H*.

Due to the nature of equation (17), increasing H* signifies increasing liquid height. The findings from previous sections can be observed in figure 30. At a low heat flux of 36W/cm^2, the H* corresponding to lower liquid heights exhibit better performance than high liquid heights except for 2mm liquid height, which observed very unstable boiling due to comparable liquid height bubble diameter.

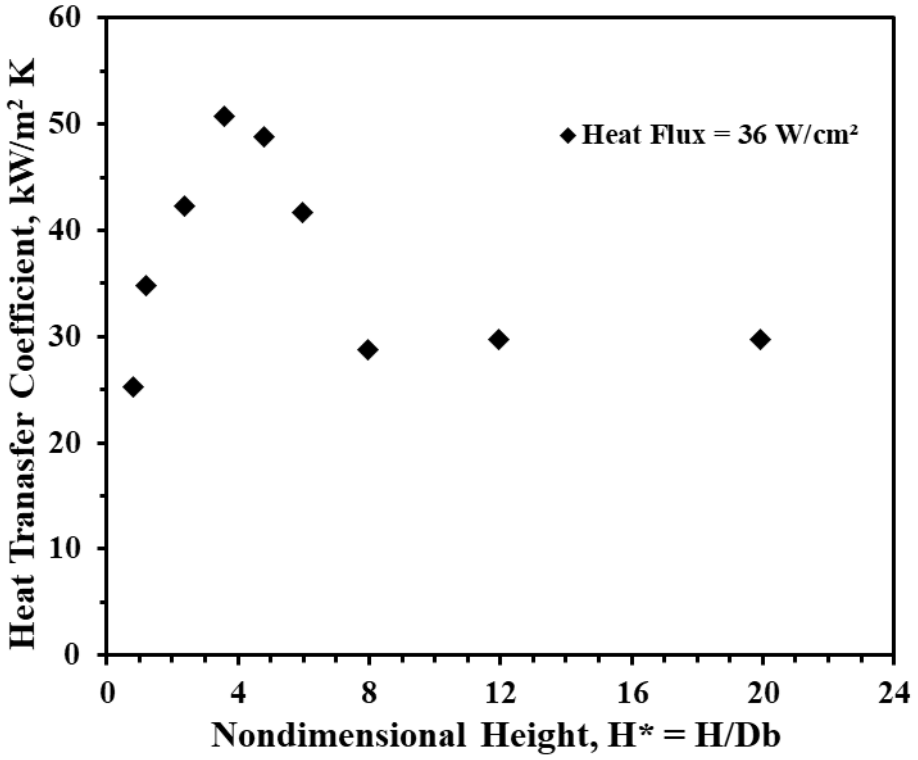

*Figure 30 Relationship between HTC and Non- D*imensionalized *Height, H*= H/Db*

As indicated by previous results, the heat transfer coefficient corresponding to higher liquid heights shows a lower heat transfer coefficient at lower heat fluxes. This observation can be well justified by the distance a vapor bubble needs to travel before effectively dumping heat into the

atmosphere. Therefore, it can be concluded that the maximum heat transfer coefficient may be achieved in a pool boiling experiment when the liquid height is about four times the bubble diameter.

7.5 Discussion

From the pool boiling experiments, it was noted that with reducing liquid height, CHF reduces. Also, it was observed that the relation between departing bubble diameter and liquid height affects the boiling performance due to change in bubble venting mechanism. High-speed video analysis uncovers two distinct vapor bubble movement mechanisms. One vapor bubble movement mechanism is observed at liquid height lower than 3x bubble diameter and it improves the HTC. The other mechanism works to improve CHF and occurs at liquid height greater than 3x bubble diameter. Non-dimensionalizing liquid height with departing vapor bubble diameter shows that maximum HTC is observed when the liquid height is 4 times the departing vapor bubble diameter.

8.0 Conclusion

Pool boiling experiments on plain copper heating chips are conducted at liquid heights of 2mm, 3mm, 6mm, 9mm, 12mm, 15mm, 20mm, 30mm, and 50mm. An experimental setup was developed along with an external reservoir to maintain liquid height during the entire pool boiling experiment at atmospheric pressure to study the effect of the height of the liquid level above the heater surface in pool boiling heat transfer. Heat input was increased slowly, and experiments were conducted up to critical heat flux (CHF) condition.

It was observed that CHF decreases as liquid height reduces from 20 mm to 2 mm. Beyond 20 mm of liquid height, CHF was observed at around 125 W/cm^2 and 20°C. Experiments with lower liquid heights showed a greater heat transfer coefficient (HTC) than experiments with higher liquid heights.

To understand the underlying bubble venting mechanism at different liquid heights, high-speed videos were recorded during the pool boiling experiment at 2000 fps at a heat flux of about 30 W/cm^2. In the case of lower liquid heights, it was observed that the expanding vapor bubbles formed a trunk-like structure to dump the heat into the atmosphere, resulting in decreased rewetting of the heating surface. The coalescing vapor bubbles also formed a foam-like layer atop the heating surface, which resulted in a reduction of CHF for surfaces with lower liquid heights. A maximum HTC of 65 kW/m^2K was observed for the plain copper surface with 12 mm liquid height, showing at least 25% enhancement in HTC than a liquid height 20 mm and beyond. The least CHF of about 67 W/cm^2 was observed for 2 mm liquid height at wall superheat of about 18°C. In higher liquid heights, vapor bubble detachment was observed from the heating surface, which allowed the rewetting of the heater surface, resulting in improved CHF than lower liquid heights.

In this work, an additional non-dimensional number was developed to represent liquid height as a function of departing vapor bubble diameter. The departing vapor bubble diameter can be defined as a characteristic length of the pool boiling process, and defining the liquid height allows understanding the liquid height in terms of departing vapor bubble diameter. When the liquid height to departing bubble diameter ratio is less than 4, the liquid height offers less resistance for the vapor bubble to vent, making the venting process more efficient. Maximum HTC was observed when the ratio is about 4. When the ratio of liquid height to bubble diameter is greater than 4, bubble detachment improves CHF.

9.0 Future Work

Conducting this study has opened opportunities for more research. The influence of liquid height on pool boiling heat transfer can be attributed to the vapor bubble's movement within the liquid bulk. Therefore, future work encircling the area mentioned above would yield a significant contribution to the scientific community.

- Further independent research can be conducted wherein the escaping bubble diameter is altered to confirm the relationship between the departing bubble diameter and liquid height. One of the ways of doing it is by creating porous heating chips.
- Moreover, extensive time study tests can be conducted on the bubble venting mechanism using high-speed video analysis. Such studies can help to break down different phases in the bubble venting process and provide further insight into the interval required to complete the whole process.
- Another exciting area of further work is to conduct pool boiling tests on a plain copper heating chip at various liquid height using different working fluids. Such tests can provide crucial information in the application of these working fluids.

Reference

[1] Incropera, F. P., and DeWitt, D. P., 2002, Fundamentals of Heat and Mass Transfer, J. Wiley, New York.

[2] Nukiyama, S., 1966, "The Maximum and Minimum Values of the Heat Q Transmitted from Metal to Boiling Water under Atmospheric Pressure," International Journal of Heat and Mass Transfer, 9(12), pp. 1419–1433.

[3] Matsuoka, H., and Urakawa, K., 1952, "Effect of the Low Water Level on Heat Transfer of Nucleate Boiling on Horizontal Heating Surface," Transactions of the Japan Society of Mechanical Engineers, 18(76), pp. 33–36.

[4] Nishikawa, K., Kusuda, H., Yamasaki, K., and Tanaka, K., 1967, "Nucleate Boiling at Low Liquid Levels," Bulletin of JSME, 10(38), pp. 328–338.

[5] Kwark, S. M., Amaya, M., Kumar, R., Moreno, G., and You, S. M., 2010, "Effects of Pressure, Orientation, and Heater Size on Pool Boiling of Water with Nanocoated Heaters," International Journal of Heat and Mass Transfer, 53(23–24), pp. 5199–5208.

[6] Rishi, A. M., Gupta, A., and Kandlikar, S. G., 2018, "Improving Aging Performance of Electrodeposited Copper Coatings during Pool Boiling," Applied Thermal Engineering, 140, pp. 406–414.

[7] A Jaikumar, and SG Kandlikar, 2015, "Enhanced Pool Boiling Heat Transfer Mechanisms for Selectively Sintered Open Microchannels | Elsevier Enhanced Reader"

[8] Cooke, D., and Kandlikar, S. G., 2010, "Pool Boiling Heat Transfer and Bubble Dynamics Over Plain and Enhanced Microchannels," p. 10.

Appendix A

The volume fraction is defined as the relation between the volume in the assembly housing and the external beaker's volume.

The volume of liquid bulk inside the setup can be calculated using the following equation.

$$V_s = V_T - V_b$$

Where,

V_s = Volume of bulk liquid inside setup

V_t = Total volume occupied by height

V_b = Volume occupied by chip and garolite block

Now, the total volume occupied for given height and volume occupied by chip and garolite block can be calculated as follows:

$$V_t = L_t \times W_t \times H_t$$

$$V_b = L_b \times W_b \times H_b$$

Substituting values into the equation above, we get:

$$V_t = 78.5\ mm \times 50\ mm \times 20\ mm$$

$$\therefore\ V_t = 78{,}500\ mm^3$$

$$V_b = 48\ mm \times 48\ mm \times 16\ mm$$

$$\therefore V_b = 13{,}824\ mm^3$$

Hence, the volume of liquid bulk inside the setup can be calculated as:

$$V_s = 78{,}500\ mm^3 - 13{,}824\ mm^3$$

$$\therefore V_s = 64{,}676\ mm^3$$

Where,

L_t = Total length

W_t = Total width
H_t = Total height
L_b = Length of garolite length
W_b = Width of garolite block
H_b = Height of garolite block quoting the volume occupied by liquid bulk inside the setup for given height with volume inside the cylinder will provide the appropriate height.

$$\therefore V_s = V_c$$

Now, the volume inside the cylinder can be found out using the following formula.

$$V_c = \pi r^2 H_c$$

Where,

V_c = Volume of liquid bulk inside the cylinder
H_c = Height of liquid bulk inside the cylinder
r = inner radius of the cylinder

$$\therefore 64{,}676\ mm^3 = \pi \times (60\ mm)^2 \times H_c$$

$$\therefore H_c = 5.7188\ mm$$

Now that relevant height present in the cylinder for the given amount of volume is found, height fraction can be found to come up with a factor to multiply the height of volume bulk inside setup and height in the cylinder

$$\frac{H_s}{H_C} = \frac{20}{5.7188}$$

$$\therefore \frac{H_s}{H_C} = 3.4972$$

Hence, the height factor between cylinder and setup is equal to 3.4972.

$$\therefore H_C = \frac{H_s}{3.4972}$$

$$\therefore H_s = 3.4972\ H_C$$

Hence, it can be concluded that the height of liquid bulk inside the setup increases by almost 3.5 times for a similar increment in the height of liquid bulk in the cylinder. Therefore, the height inside the setup can easily be met using the siphon method to feed the liquid level.

Appendix B

The heating chip surface temperature cannot be calculated without establishing 1D heat conduction across the copper heating chip. One way to ensure 1D heat conduction is by calculating the temperature drop between two adjacent thermocouples. In the LabView program, the temperature drop is monitored through a measure called 'Spacing.' It is the ratio between the difference between T_2 and T_1 and T_3 and T_2. Spacing can be defined as follows:

$$Spacing = \frac{(T_2 - T_1)}{(T_3 - T_2)}$$

Prior to recording the temperatures T1, T2, and T3, a spacing of 1 is ensured and stabilized for a period of 10 seconds. Thus, satisfying Fourier's 1D conduction law.

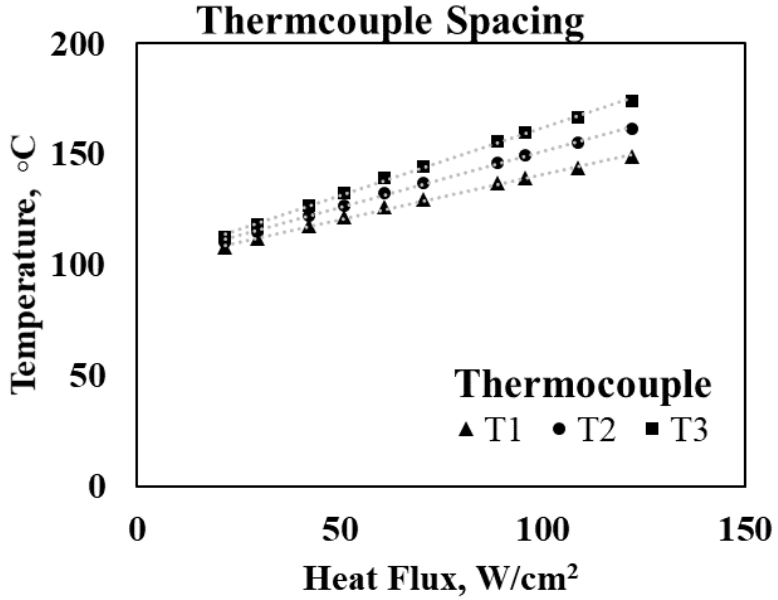

Figure 31 Thermocouple Spacing for 1D conduction

Figure 31 shows temperature readings from T_1, T_2, and T_3 thermocouples for each recorded data point during the experiment at 15 mm liquid height. Each dataset is fitted with a linear trend line, and the table below shows the corresponding equation of line and agreement.

Thermocouple	**Equation**	**R^2**
T_1	y = 0.4049x + 100.23	0.9967
T_2	y = 0.5106x + 100.26	0.9979
T_3	y = 0.6154x + 100.34	0.9985

The high value of R^2 shows the substantial agreement of the fitted model with the given data points. A similar approach was used to determine the 1D conduction of heat across the copper heating chip for all given experiments.